Mechanical stimulation induces rapid fibroblast proliferation and accelerates the early maturation of human skin substitutes

Wahlsten, Adam ; Rütsche, Dominic ; Nanni, Monica ; Giampietro, Costanza ; Biedermann, Thomas ; Reichmann, Ernst ; Mazza, Edoardo

Abstract: The clinical treatment of large, full-thickness skin injuries with tissue-engineered autologous dermo-epidermal skin substitutes is an emerging alternative to split-thickness skin grafting. However, their production requires about one month of in vitro cell and tissue culture, which is a significant drawback for the treatment of patients with severe skin defects. With the aim to reduce the production time, we developed a new dynamic bioreactor setup that applies cyclic biaxial tension to collagen hydrogels for skin tissue engineering. By reliably controlling the time history of mechanical loading, the dynamic culturing results in a three-fold increase in collagen hydrogel stiffness and stimulates the embedded fibroblasts to enter the cell cycle. As a result, the number of fibroblasts is increased by 75% compared to under corresponding static culturing. Enhanced fibroblast proliferation promotes expression of dermal extracellular matrix proteins, keratinocyte proliferation, and the early establishment of the epidermis. The time required for early tissue maturation can therefore be reduced by one week. Analysis of the separate effects of cyclic loading, matrix stiffening, and interstitial fluid flow indicates that cyclic deformation is the dominant biophysical factor determining fibroblast proliferation, while tissue stiffening plays a lesser role. Local differences in the direction of deformation (in-plane equibiaxial vs. uniaxial strain) influence fibroblast orientation but not proliferation, nor the resulting tissue properties. Importantly, dynamic culturing does not activate fibroblast differentiation into myofibroblasts. The present work demonstrates that control of mechanobiological cues can be very effective in driving cell response toward a shorter production time for human skin substitutes.

DOI: https://doi.org/10.1016/j.biomaterials.2021.120779

DOI: https://doi.org/10.1016/j.biomaterials.2021.120779

Biomaterials 273 (2021) 120779

Contents lists available at ScienceDirect

Biomaterials

journal homepage: www.elsevier.com/locate/biomaterials

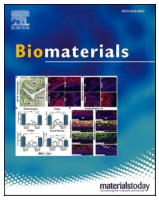

Mechanical stimulation induces rapid fibroblast proliferation and accelerates the early maturation of human skin substitutes

Adam Wahlsten [a,1], Dominic Rütsche [b,c,1], Monica Nanni [a,b,c], Costanza Giampietro [a,d], Thomas Biedermann [b,c], Ernst Reichmann [b,c,*], Edoardo Mazza [a,d,**]

[a] Institute for Mechanical Systems, Department of Mechanical and Process Engineering, ETH Zurich, Leonhardstrasse 21, 8092 Zurich, Switzerland
[b] Tissue Biology Research Unit, Department of Surgery, University Children's Hospital Zurich, Wagistrasse 12, 8952 Schlieren, Switzerland
[c] Children's Research Center, University Children's Hospital Zurich, Steinwiesstrasse 75, 8032 Zurich, Switzerland
[d] Empa, Swiss Federal Laboratories for Materials Science and Technology, Überlandstrasse 129, 8600 Dübendorf, Switzerland

ARTICLE INFO

Keywords:
Dynamic bioreactor
Human dermal fibroblast
Keratinocyte
Proliferation
Skin substitute
Tissue engineering

ABSTRACT

The clinical treatment of large, full-thickness skin injuries with tissue-engineered autologous dermo–epidermal skin substitutes is an emerging alternative to split-thickness skin grafting. However, their production requires about one month of *in vitro* cell and tissue culture, which is a significant drawback for the treatment of patients with severe skin defects. With the aim to reduce the production time, we developed a new dynamic bioreactor setup that applies cyclic biaxial tension to collagen hydrogels for skin tissue engineering. By reliably controlling the time history of mechanical loading, the dynamic culturing results in a three-fold increase in collagen hydrogel stiffness and stimulates the embedded fibroblasts to enter the cell cycle. As a result, the number of fibroblasts is increased by 75% compared to under corresponding static culturing. Enhanced fibroblast proliferation promotes expression of dermal extracellular matrix proteins, keratinocyte proliferation, and the early establishment of the epidermis. The time required for early tissue maturation can therefore be reduced by one week. Analysis of the separate effects of cyclic loading, matrix stiffening, and interstitial fluid flow indicates that cyclic deformation is the dominant biophysical factor determining fibroblast proliferation, while tissue stiffening plays a lesser role. Local differences in the direction of deformation (in-plane equibiaxial vs. uniaxial strain) influence fibroblast orientation but not proliferation, nor the resulting tissue properties. Importantly, dynamic culturing does not activate fibroblast differentiation into myofibroblasts. The present work demonstrates that control of mechanobiological cues can be very effective in driving cell response toward a shorter production time for human skin substitutes.

1. Introduction

As the outermost and largest organ of the human body, the skin constitutes the essential barrier that protects us against various threats, such as physical damage, interstitial fluid loss, and infections. In case of large (>30% body surface area), full-thickness wounds, *e.g.* due to severe burns, the loss of both dermal and epidermal compartments presents a serious problem because of the insufficient self-healing capability and the limited availability of split-thickness autologous skin for transplantation [1,2]. While rapid epithelialization is important to re-establish essential functions of the skin, such as the epidermal barrier, the reconstruction of the dermis is essential for optimized wound healing as well as a functional and aesthetic outcome [1,2]. In fact, in case of full-thickness wounds, tissue regeneration with minimal scarring depends on the cellular signaling between dermis and epidermis in a reciprocal manner [3]. Since the 1980's, tissue-engineered dermo–epidermal skin grafts have been investigated and developed in research laboratories (*e.g.* [4–8]) and can be engineered to achieve near-normal anatomical and functional properties. As these skin grafts become increasingly accessible, they promise to eliminate problems associated with split-thickness skin

* Corresponding author. Tissue Biology Research Unit, Department of Surgery, University Children's Hospital Zurich, Wagistrasse 12, 8952 Schlieren, Switzerland.
** Corresponding author. Institute for Mechanical Systems, Department of Mechanical and Process Engineering, ETH Zurich, Leonhardstrasse 21, 8092 Zurich, Switzerland.
E-mail addresses: Ernst.Reichmann@kispi.uzh.ch (E. Reichmann), mazza@imes.mavt.ethz.ch (E. Mazza).
[1] These authors contributed equally and share first authorship of this work.

https://doi.org/10.1016/j.biomaterials.2021.120779
Received 8 July 2020; Received in revised form 28 February 2021; Accepted 20 March 2021
Available online 27 March 2021

transplantation, for example donor-site shortage and scarring due to the insufficient dermal support [2,9].

Over the last decade, we have developed and established dermo–epidermal skin substitutes based on collagen type I hydrogels in *in vitro* and preclinical studies [5,10–13]. Recently, we successfully applied large, GMP-produced, autologous dermo–epidermal skin grafts in a Phase I clinical trial [14], and a multicenter Phase II study is ongoing. While the functionality of the skin grafts was thus demonstrated, the production of these grafts for clinical transplantation requires four to five weeks of *in vitro* culturing, and reducing the production time still represents a major challenge [14]. Our production process consists of three principal steps: (i) isolation and 2D expansion (~ two weeks) of dermal fibroblasts (FBs) and keratinocytes (KCs) from a skin biopsy; (ii) embedding and culturing of FBs in a plastically compressed collagen hydrogel (~ one week); and (iii) cultivation of KCs on top of this dermal matrix until they completely cover the surface and have formed an initial epidermis (~ one week) [14,15]. In fact, the long cultivation time required is a common drawback for autologous dermo–epidermal skin substitutes: other reports on the time from biopsy extraction to skin substitute transplantation range from five weeks [16] up to nine weeks [17]. For patients suffering from large burn wounds, this corresponds to long waiting times until transplantation. Reducing the overall *in vitro* culturing time without compromising skin graft quality thereforerepresents an essential step toward improved outcome for these patients.

A potential method to accelerate the maturation of tissue-engineered grafts is to use dynamic bioreactor systems [18,19]. In particular, bioreactors applying controlled mechanical loading to the grafts leverage the cell mechanosensitive response [20,21] to stimulate, for example, cell proliferation, differentiation, and extracellular matrix (ECM) deposition. Examples can be found in tissue engineering of cardiovascular constructs [22–24], smooth muscle tissue [25], tendon [26], cartilage [27,28], and skin [29,30]. Although less pronounced when compared to arteries or tendons, physiological deformations occur in skin associated with body movements. Furthermore, skin stretch is known to stimulate tissue growth through cell proliferation and deposition of new ECM, and this principle is exploited in reconstructive surgery [31]. More generally, tissue stretching is directly coupled with several changes in the physicochemical properties of the ECM [32,33], and the effects of individual biophysical factors on cell behavior, such as matrix stiffening [34–36] and interstitial fluid flow [37,38], are only beginning to be understood.

Here, we demonstrate that application of cyclic mechanical loading can accelerate the production of human dermo–epidermal skin substitutes. We present a novel dynamic bioreactor system for skin tissue engineering, which allows exposing large (30 mm diameter), FB-containing native collagen hydrogels to pressure-controlled cyclic membrane inflation, resulting in equibiaxial and uniaxial strain in the center and the rim of the gels, respectively. After three days of cyclic loading, the bioreactor-treated dermal substitutes exhibited a three-fold increase in material stiffness due to corresponding thinning of the hydrogels. In contrast to static culture where FBs remained quiescent, dynamic culturing induced FBs to enter the cell cycle and to proliferate rapidly, yielding a 75% increase in cell number independent of the state of strain. The dynamically cultured dermal substitutes were shown to support faster KC proliferation and faster establishment of an early epidermis compared to corresponding statically cultured dermal matrices. The influence of matrix stiffness, interstitial fluid flow, and strain directionality on FB proliferation is discussed, providing a mechanobiological understanding of the accelerated tissue maturation.

2. Materials and methods

2.1. Bioreactor design

The dynamic bioreactor was designed based on a mechanical testing setup previously employed for equibiaxial characterization of soft elastomers and biological tissues [39,40]. The bioreactor features an inflation chamber, which is connected using gas-permeable silicone tubing to a syringe pump (PHD Ultra, Harvard Apparatus) and a pressure sensor (MPX 4250 AP, Freescale), see Fig. 1. To ensure safe and reliable long-term cyclic loading of soft hydrogels, custom corrugated clamps with interlocking circular grooves were developed (Fig. 1ce), inspired by a design previously used for fracture testing of soft elastomers [41]. After fastening the bioreactor chamber inside an acrylic glass container, the hydrogel is clamped and the clamps are secured to the inflation chamber using stainless steel screws (Fig. 1d). Thereafter, the acrylic glass container is filled with cell culture medium to fully cover the hydrogel, closed with a lid, and placed inside an incubator (Galaxy 48 R, Eppendorf) to provide controlled environmental conditions (37 °C, 5% CO_2), and the tubes are connected to the syringe pump and the pressure sensor. The clamps were 3D-printed (Objet 500 Connex, Stratasys) using the acrylic polymer VeroWhitePlus (Stratasys), whereas the other parts were machined out of polyoxymethylene (POM) or polyethylene terephthalate (PET).

2.1.1. Mechanical actuation

Mechanical actuation is achieved by controlling the time history of the inflation pressure p (Fig. 1a). A custom-written Matlab (R2018b, The Mathworks, Inc.) code and user interface reads the current pressure value and updates the syringe pump flow rate in a proportional-integral-derivative (PID) feedback control loop. For dynamic culturing experiments, a sinusoidal target pressure signal is prescribed so that the inflation pressure oscillates between a maximum p_{max} and a minimum p_{min} at the frequency f. Frequencies up to 0.2 Hz were tested in preliminary experiments. The bioreactor operation is fully automatized and can be interrupted for medium change.

By controlling the inflation pressure, neither the strain nor the membrane tension is prescribed, but instead the bioreactor imposes a time-variable loading history on the hydrogel membrane. In fact, strain and membrane tension change over time as determined by the mechanical properties of the hydrogel. Due to the clamping constraint, the circumferential strain vanishes at the rim, whereas the radial strain is positive. In the center, both membrane strains are equal. The heterogeneous strain field imposed thus allows for investigating differences in cell and tissue response with respect to strain directionality, *cf.* Fig. 2g.

2.1.2. Bioreactor characterization

Measurements of the actual strains during bioreactor operation were performed on acellular analogs of the dermal substitutes under non-sterile conditions at room temperature, using a physiological saline solution (0.15 M NaCl) as infusing medium. An ink pattern was applied in the center of the gel with a waterproof pen (GeoCollege Pigment Liner 0.1) to facilitate optical strain analysis. The monotonic behavior of the acellular hydrogels was assessed by slowly (0.1 kPa s^{-1}) inflating the membrane up to a pressure of 15 kPa; this served as a basis for selecting the maximum pressure to be applied during dynamic culturing. The evolution of equibiaxial strain during cyclic loading was assessed over more than 1000 cycles at $f = 0.1$ Hz and at the chosen maximum pressure $p_{max} = 1.5$ kPa. For this experiment, the bioreactor operation was synchronized with top-view image acquisition using a CMOS camera (EO-2323 Monochrome, Edmund Optics) equipped with a telecentric lens (NT55-349, Edmund Optics). The in-plane principal stretches λ_1 and λ_2 in the center of the gel were extracted from the image sequence using a custom-written optical flow tracker [40], and the equibiaxial strain was computed as $\varepsilon_{eb} = \sqrt{\lambda_1 \lambda_2} - 1$. Fiducial points for tracking were identified based on the applied ink pattern in a small circular region (3 mm radius) around the apex (Supplementary Fig. S1).

The cyclic behavior of acellular dermal substitutes was further analyzed in uniaxial tension experiments, where precise displacement- and force-controlled loading conditions can be applied. Briefly, test-

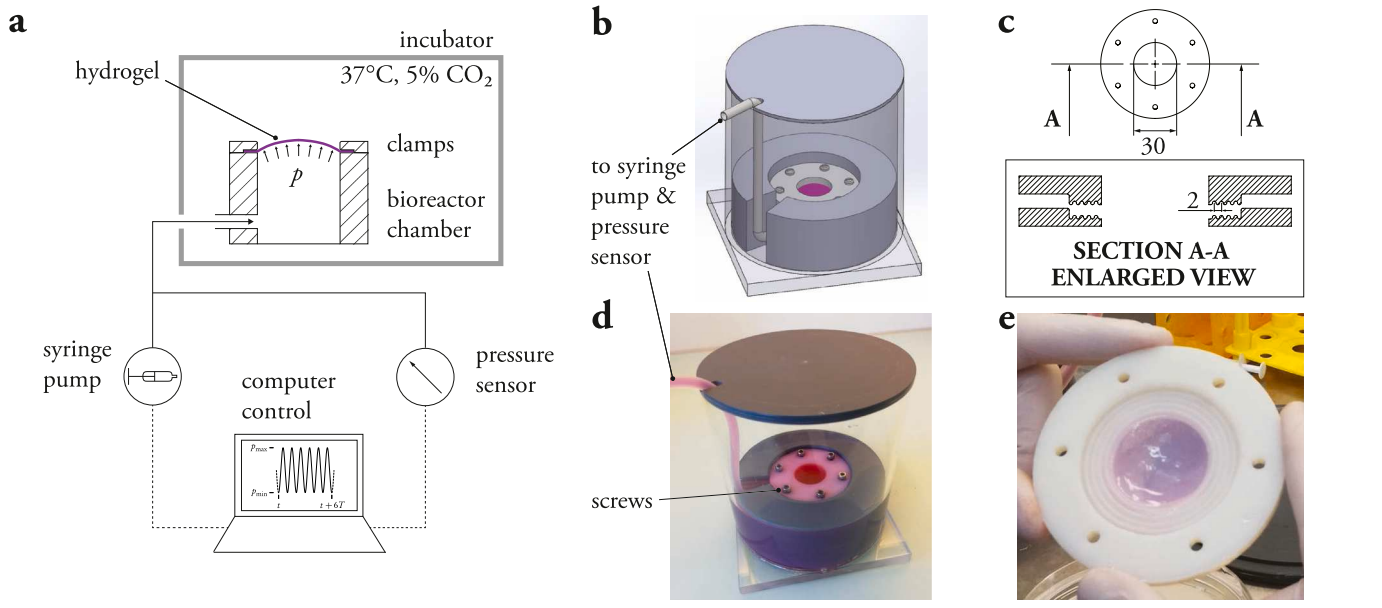

Fig. 1. Dynamic bioreactor for skin tissue engineering. (**a**) A computer-controlled feedback loop adjusts the syringe pump actuation to cyclically modulate the pressure p on a hydrogel, which is clamped on top of an inflation chamber. The bioreactor design (**b**) and realization (**d**) are shown, with corrugated clamps (**c**, **e**) ensuring reliable and gentle clamping conditions over three days of continuous cyclic loading. Dimensions in **c** are in mm.

pieces were cut to 40 mm × 5 mm (gauge dimensions: 20 mm × 5 mm) and clamped to a custom-built testing setup (MTS Systems) consisting of horizontal hydraulic actuators equipped with 50 N force sensors [33,40]. Displacement-controlled cyclic loading was prescribed between a reference state, defined by a small threshold force close to sensor resolution (0.005 N), and a nominal strain of 10% at a displacement rate of 0.02 mm s^{-1}. For comparison, a cyclic force-controlled test was performed up to a force of 0.12 N, chosen as the peak force reached in the first displacement-controlled cycle. The local in-plane principal stretches λ_1 and λ_2 were extracted from top-view images taken with a CCD camera (Pike F-100B, Allied Vision Technologies) equipped with a telecentric lens (NT55-349, Edmund Optics) using the optical flow tracking method [40] as described above.

2.2. Dynamic bioreactor experiments

A series of dynamic culturing experiments were performed to assess the effects on tissue properties and cell behavior, as described in this section, summarized in Table 1, and illustrated in Fig. 2.

2.2.1. Cell isolation and culture

Tissue biopsies were provided by the University Children's Hospital Zurich. All human primary cells were isolated from human back skin obtained from three donors between the ages one and ten. All patients' parents gave consent for the usage of the skin samples; the use of skin biopsies for research purposes had been approved by the Ethical Committee of Canton Zurich (BASEC-Request-Nr. 2018-00269). Biopsies were stored in Dulbecco's Modified Eagle Medium (DMEM; Gibco) supplemented with 1.5 µl ml^{-1} gentamycin (10 mg ml^{-1}, Sigma) and 30 µl ml^{-1} penicillin–streptomycin (10,000 U ml^{-1} penicillin, 10 mg ml^{-1} streptomycin; Sigma). FBs and KCs were separately isolated and cultured as previously described [42]. Briefly, skin samples were incubated overnight in 5 ml diluted dispase (2.5 ml dispase: 50 U ml^{-1}, Corning; 2.5 ml Dulbecco's phosphate-buffered saline (DPBS); 500 µl gentamycin), after which dermis and epidermis were mechanically separated.

Separated dermal parts were minced and incubated for 30 min at 37 °C in 5 ml collagenase (collagenase G + H, Abiel; 10 µl ml^{-1} in DPBS). Digestion efficiency was increased by mixing every 10 min. Afterwards, the dermis was dissociated by pipetting up and down. The reaction was stopped by adding 3 volume equivalents of $DMEM^{+++}$ (DMEM low glucose (Gibco) supplemented with 100 µl ml^{-1} fetal bovine serum (FBS; Gibco), 10 µl ml^{-1} penicillin–streptomycin, and 10 µl ml^{-1} of 1 M HEPES (Gibco)). The cell suspension was passed through a 100 µm cell strainer. Finally, cells were spun down (10 min at 1250 rpm), resuspended in $DMEM^{+++}$, and plated on 10 cm dishes containing 10 ml $DMEM^{+++}$. Cells were grown in a humidified atmosphere at 37 °C and 5% CO_2. During the first four days after isolation, culture plates were washed daily with concurrent medium change. Afterwards, the cell culture medium was only changed every second day. Passaging of FB cultures was carried out at 70%–80% confluence.

Epidermal parts were digested for 2 min at 37 °C in a Falcon tube containing 2 ml prewarmed trypsin/EDTA 10×. Following mixing every 30 s, the digestion was stopped by adding one volume equivalent $DMEM^{+++}$, and the solution was passed through a 100 µm cell strainer. The filtrate was spun down (5 min, 950 rpm), and the resulting pellet was resuspended in CellnTec-57 medium, containing supplements A, B, C, and BPE from the CnT-57.S supplement pack (CELLnTEC Advanced Cell Systems). Cells were counted and plated at 2 to 3 million cells per 10 cm dish. Dishes for KC culturing were previously coated with acidified type I soluble collagen (5 mg ml^{-1}; Symatese) in DPBS (ratio 1:50). During the first four days after isolation, culture plates were washed daily with concurrent medium change. Afterwards, the cell culture medium was only changed every second day. Passaging of KC cultures was carried out at 70%–80% confluence.

2.2.2. Dermal substitute production

The procedure for the fabrication of collagen type I hydrogels is based on a previously published protocol for the production of stable, plastically compressed hydrogels [5]. Briefly, cultured FBs were harvested at passage 3. 1×10^7 cells were resuspended in 4 ml $DMEM^{+++}$ and subsequently mixed with neutralizing buffer and acidified type I soluble collagen (5 mg ml^{-1}; Symatese) to obtain a 30 ml hydrogel mixture with a final cell concentration of $3.3 \times 10^5 ml^{-1}$. The mixture was immediately poured into 6 cm × 6 cm custom-made culture inserts (Oxyphen AG; 5 µm pore size) and transferred into an incubator (37 °C, 5% CO_2, 45 min) to allow for gel clotting. Hydrogels were compressed to 1 mm final thickness over a time period of 1 h using a fully computerized

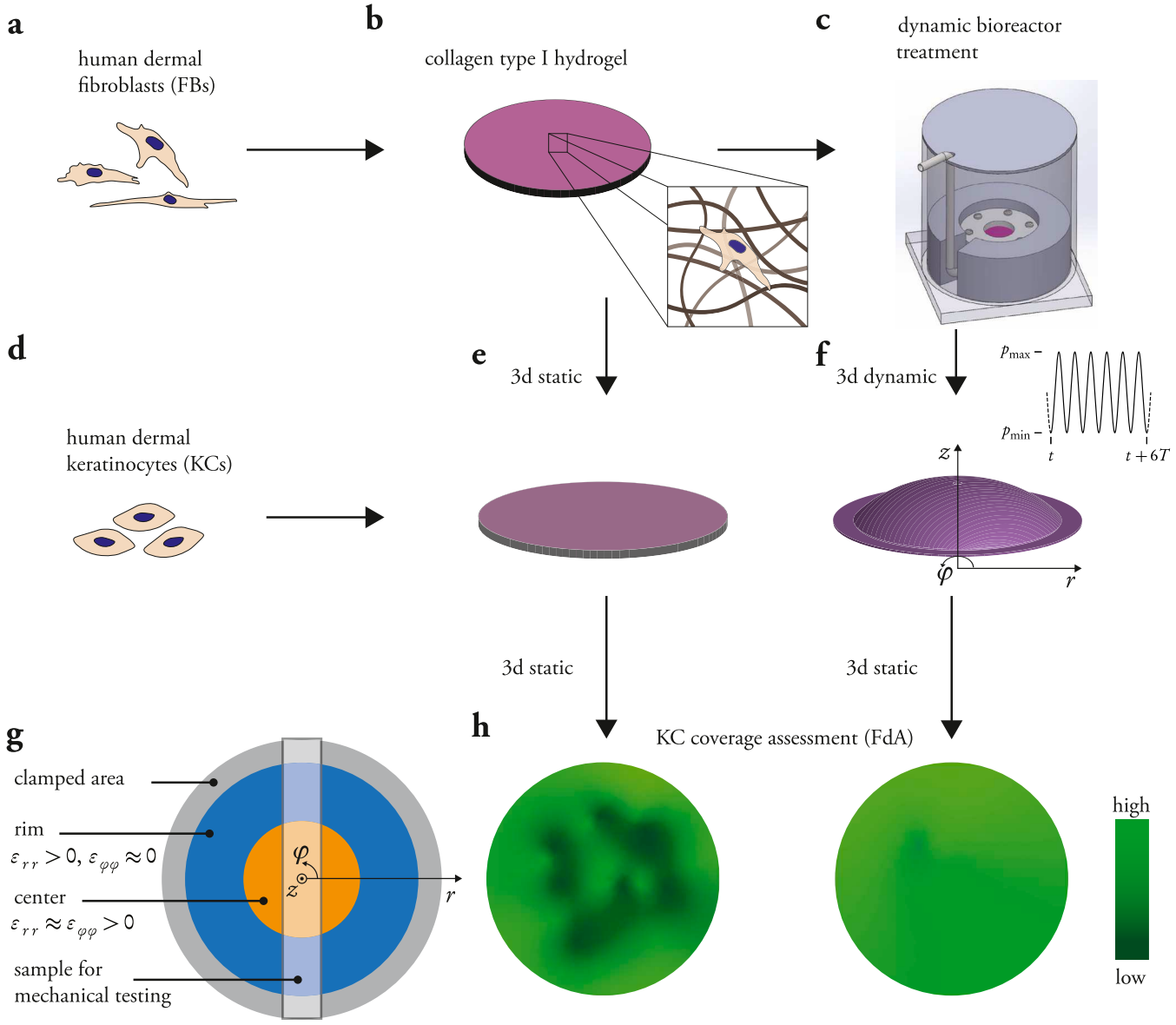

Fig. 2. Illustration of the dynamic culturing experiments. Primary human dermal fibroblasts (FBs) (**a**) and keratinocytes (KCs) (**d**) were isolated from skin biopsies, and FBs were embedded in plastically compressed collagen type I hydrogels (**b**). The hydrogels were either exposed to dynamic culturing (**c**, **f**) or kept in static culture for three days (**e**). Cultured gels were either analyzed for mechanical properties and cell behavior (**g**), or seeded with KCs and statically cultured for 3 more days. Thereafter, the early maturation of dynamically and statically cultured dermo–epidermal skin substitutes was assessed, for example by analyzing KC coverage using fluorescein diacetate (FdA) live staining (**h**).

Table 1
Summary of the experimental conditions in terms of static preculture with fibroblasts, dynamic bioreactor treatment, and static postculture with keratinocytes (KCs). Three independent experiments per condition were performed.

Condition	Static (pre)	Dynamic	Static (post)	Total time
3d static	3d	–	–	–
3d dynamic	–	3d	–	–
7d static	7d	–	–	–
3d static + 3d KC static	3d	–	3d	6d
3d dynamic + 3d KC static	–	3d	3d	6d
7d static + 3d KC static	7d	–	3d	10d

compression device (in-house developed; unpublished data). To create hydrogels of further increased stiffness, gels were compressed overnight by means of a weight and a custom-made stamp, with inserts of prescribed thickness (0.5 mm or 0.25 mm) controlling the level of compaction.

2.2.3. Dynamic culturing of dermal substitutes

Dynamic bioreactor experiments were performed under sterile conditions in a humidified atmosphere at 37 °C and 5% CO_2 with $DMEM^{+++}$ as infusing and culturing medium. All bioreactor components were sterilized by autoclave treatment or by repeated washes in 70% EtOH and subsequent rinsing in distilled water and PBS. Dermal substitutes were exposed to three days of continuous cyclic loading at $f = 0.1$ Hz with a maximum pressure $p_{max} = 1.5$ kPa (Fig. 2cf). A minimum pressure $p_{min} = 0.1$ kPa was set to avoid the gel becoming slack at the end of the cycle. Static controls were kept in tissue culture flasks in identical medium and environmental conditions as the dynamically cultured gels.

After three days, the dynamically treated dermal substitutes were

extracted for analysis of their structural and material properties and cell behavior. FB viability was assessed by fluorescein diacetate–propodium iodide (FdA–PI) live staining [43]. A central strip of 5 mm width and approximately 50 mm length was cut for mechanical testing (Sec. 2.2.5), see Fig. 2g; the remaining material was used for biological assays (Sec. 2.2.6 to 2.2.8).

2.2.4. Keratinocyte seeding and culture

To analyze whether the dynamically cultured dermal substitutes could support KCs to form an epidermis, the dermal substitutes were first cultured in the dynamic bioreactor for three days as described above. Thereafter, they were taken out of the bioreactor but kept attached in the clamps to remain fixed and homogeneously seeded with KCs at a density of $1.5 \times 10^5 \mathrm{cm}^{-2}$, see Fig. 2cfd. After KC seeding, the dermal matrices with KCs were maintained in static culture for three days. Corresponding static controls were seeded with KCs at day three or day seven post dermal substitute preparation (cf. Table 1), for which previous results had shown that a minimum of six days of FB preconditioning of the dermal matrix was necessary for successful KC surface coverage [15]. Note that KCs were seeded at a sufficient density to quickly be able to form a monolayer if able to adhere to the surface. KC viability and confluency were determined by fluorescein diacetate (FdA) live cell staining following published protocols [43,44]. Briefly, a 0.6 mM stock solution of FdA in acetone was diluted 1000× in PBS, and 2 ml of the 0.6 μM FdA staining solution was added onto the gel. Fluorescence was checked after 2 min using a Nikon SMZ1500 zoom stereomicroscope with epi-fluorescence attachment (P-FLA2), and the complete gel surface was imaged three days post KC seeding to assess viability and coverage.

KC surface coverage was quantified from the acquired FdA image by applying an adaptive Gaussian threshold followed by a morphological closing operation using Python (version 3.7.6, Python Software Foundation) bindings for the open source computer vision library OpenCV (version 3.4.2, [45]). After segmentation, the KC coverage was evaluated as the percentage of covered pixels relative to the total surface area.

2.2.5. Mechanical testing

The mechanical properties of static controls and dynamically cultured dermal substitutes were assessed immediately after completed static/dynamic culturing. Testpieces for uniaxial tension tests were cut to 50 mm × 5 mm (gauge dimensions: 40 mm × 5 mm), see Fig. 2g. For the dynamically treated samples, this large aspect ratio allows for a large central sample region in a state of uniaxial tension, including both the center and the rim. One loading–unloading cycle was performed up to 15% nominal strain at a nominal strain rate of 0.1% s^{-1} in the testing setup described above (Sec. 2.1.2). All mechanical tests were performed at room temperature with samples immersed in a 0.15 M NaCl bath.

Nominal tension and stress were calculated as $T = F/W$ and $P = F/(WH)$, respectively, where F is the measured force, W the reference width, and H the gel thickness. Sample dimensions and local strain were measured in both the center and the rim to obtain the region-specific mechanical properties. The reference width W was obtained from the top-view images, the gel thickness H was estimated from whole-mount immunostainings (see Sec. 2.2.6), and the local principal stretches λ_1 and λ_2 were extracted for each region separately using a custom-written optical flow tracking algorithm [40] as described above (Sec. 2.1.2). Material and membrane tangent stiffness were defined as $E = \frac{\partial P}{\partial \lambda_1}$ and $K = \frac{\partial T}{\partial \lambda_1}$, respectively, and the tangent Poisson's ratio as $\nu_{12} = -\frac{\partial \ln \lambda_2}{\partial \ln \lambda_1}$ [33,46]. For comparison between groups, these quantities were evaluated at $\lambda_1 = 1.05$; therein, reference data from uniaxial tension tests on human abdominal and breast skin from our previous work [33] were included for comparison.

2.2.6. Immunofluorescence

For immunofluorescence (IF) of cells cultured on culture plastic, cells were fixed for 5 min in an ice-cold acetone–methanol mixture (1:1, (v/v)). For stainings of cryosections, hydrogels were fixed in neutralized 4% paraformaldehyde (PFA; J.T. Baker) for 4 h at 4 °C, immersed in a 30% sucrose solution at 4 °C overnight, and infiltrated with a 50/50 30% sucrose/OCT solution for 8 h at 4 °C. Finally, the hydrogel samples were snap-frozen in liquid nitrogen. Cryosections of 15 μm thickness were fixed and permeabilized for 5 min in ice-cold acetone. Thereafter, the fixation mixture was removed and the cell/cryosection samples were dried for 30 s. After blocking for 30 min using 2% bovine serum albumin (BSA) in PBS at room temperature, the primary antibody was applied for 30 min at 37 °C. Cryosections and cells were then washed with DPBS, after which blocking and antibody incubation were repeated for the secondary antibody.

For whole-mount immunostainings, hydrogels were fixed in neutralized 4% PFA for 6 h at 4 °C and washed for at least another 6 h with PBS-TX (DPBS/0.3% Triton X-100 (Sigma)). The washing solution was exchanged every 30 min. Finally, samples were blocked for 2 h with immunomix (PBS-TX, 10% BSA, 0.05% sodium azide). Primary and secondary antibodies were applied for 12 h at 4 °C and at room temperature, respectively. Intermediate washing steps were conducted.

The following primary antibodies were used: mouse anti-Ki67 (BD Biosciences, BD550609, 1:100), rabbit anti-Ki67 (Abcam, ab15580, 1:100), mouse anti-α-SMA (Dako, M0851, clone 1A4, 1:500), mouse anti-pancytokeratin (Santa Cruz, sc-8018, 1:100), rabbit anti-E-cadherin (Invitrogen, MA5-14458, 1:100), mouse anti-CK15 (Santa Cruz, sc-56520, 1:50), rabbit anti-CK19 (Abcam, ab52625, 1:100), mouse anti-β4-integrin–Alexa Fluor 488 (Novus Biologicals, FAB4060G, 1:50), mouse anti-α6-integrin (Chemicon, CBL458, 1:50), mouse anti-collagen I (Abcam, ab6308, 1:100), rabbit anti-tropoelastin (EPC, PR398, 1:100), mouse anti-YAP (Santa Cruz, sc-101199, 1:50). The following secondary antibodies were used: donkey anti-mouse IgG H&L Alexa Fluor A488 (Abcam, ab150105, 1:400), donkey F(ab')2 anti-mouse IgG H&L Alexa Fluor A568 (Abcam, ab175699, 1:400), goat anti-rabbit IgG H&L Alexa Fluor A647 preadsorbed (Abcam, ab150083, 1:400). F-actin was visualized using TRITC-conjugated rhodamine-phalloidin (Invitrogen, R415) at final concentration of 10 μM. Cell nuclei were counterstained with Hoechst 33258 bisbenzimide (Sigma, 94403, 1:1000) or DAPI (ThermoFisher Scientific, 62248, 1:1000).

Finally, cells, cryosections, and gels were mounted using Fluoroshield histology mounting medium (Sigma, F6182). Imaging was carried out using an inverse confocal laser scanning microscope (Leica SP8) or an inverse spinning-disk confocal microscope (Nikon Ti-E).

For the evaluation of cell number and relative cell density, the total number of cells within a full-thickness z-stack (area: 580 μm × 580 μm) was counted based on nuclear staining. The thickness of the gel was determined by the region of detectable fluorescence signal. Relative cell density was calculated as total number of cells divided by the thickness. For the quantification of Ki67-positive FBs, cells were counted within an imaged area of 580 μm × 580 μm for z-stacks of ≥250 μm.

To quantify the FB alignment in the center and rim of the dynamically cultured gels, z-projections of the visualized F-actin were extracted and the in-plane orientation of actin fibers was analyzed using the OrientationJ plug-in for ImageJ [47]. The so-obtained actin fiber orientation distributions were normalized to integrate to unity, and the average over three images (one per biological replicate) was computed for each condition (3d static; 3d dynamic: center and rim). Note that the imaging in the center and the rim was performed with respect to the same radial and circumferential direction to facilitate comparison across samples. To this end, the image labeled center was acquired slightly off from the actual center, as sketched in Fig. 7e. Orientation distributions from representative images are also shown as polar histograms (bin width: 4°).

2.2.7. Nucleic acid isolation

Total RNA was isolated from encapsulated cells according to the manufacturer's protocol (RNeasy, Qiagen) with minor modifications.

Briefly, collagen gels were minced and mixed with 1 ml TRIzol (Invitrogen, 15596026). The gels were then homogenized using 20-G needles and TRIzol–gel mixtures were allowed to sit for 10 min at room temperature. Afterwards, 200 µl chloroform was added and the mixtures were shaken vigorously. Aqueous and organic phases were separated by centrifugation (15,000 g, 15 min, 4 °C). The aqueous phase containing RNA was carefully removed and mixed with an equal volume (ca. 600 µl) of 70% EtOH. 500 µl of EtOH–RNA solution was loaded onto an RNeasy mini spin column, centrifuged (15,000 g, 15 s, 4 °C), and the flow-through was discarded. The following washing steps were performed: 700 µl of buffer RW1 (15,000 g, 15 s, 4 °C); 500 µl of buffer RPE (15,000 g, 15 s, 4 °C); and 500 µl of buffer RPE (15,000 g, 2 min, 4 °C). Next, the column was placed in a collection tube and eluted using RNase-free water (15,000 g, 2 min, 4 °C). RNA purity was assessed using the Epoch spectrophotometer with Take3 micro-volume plate (BioTek) for microliter analysis. Only pure RNA with absorption ratios $A_{260}/A_{280} \sim 2.0\text{-}2.1$ and $A_{260}/A_{230} \sim 2.1\text{-}2.3$ was considered for reverse-transcription quantitative polymerase chain reaction (RT-qPCR) analysis. RNA was stored at −80 °C until further use.

2.2.8. RT-qPCR

RT-qPCR was performed according to published protocols [48–51]. First, single-stranded RNA was converted to cDNA using the GoScript Reverse Transcriptase kit (Promega) following the manufacturer's instructions. RT-qPCR was carried out in triplicates using SYBR green chemistry (PowerTrack SYBR Green, ThermoFisher). For the actual amplification steps, the StepOnePlus real-time PCR system (Applied Biosystems/ThermoFisher Scientific) was used. All data were normalized to the reference gene GAPDH and quantification was performed using the $2^{-\Delta\Delta CT}$ method with efficiency correction. The relative gene expression ratio was calculated with respect to confluent cultures of FBs that were quiescent for at least 3 days or statically cultured dermo–epidermal skin substitutes (3d static + 3d KC static). The primers used are listed in Supplementary Table S1.

2.3. Statistical analysis

Data are shown as mean ± standard deviation. Correlation between two variables was analyzed by Pearson's correlation test. Statistical comparisons between multiple groups were assessed with a one-way ANOVA followed by Tukey's HSD post-hoc test. For the RT-qPCR data, the ΔCT values were compared with respect to the reference sample (quiescent FBs in 2D culture or 3d static + 3d KC static) by one-way ANOVA and subsequent Dunnett's post-hoc test. The data on human skin were not included for statistical comparisons. Significance was determined for $P < 0.05$.

3. Results

3.1. Bioreactor characterization

The mechanical characterization of acellular dermal substitutes exposed to bioreactor loading is reported in Fig. 3. From the pressure–equibiaxial strain relationship obtained in monotonic inflation

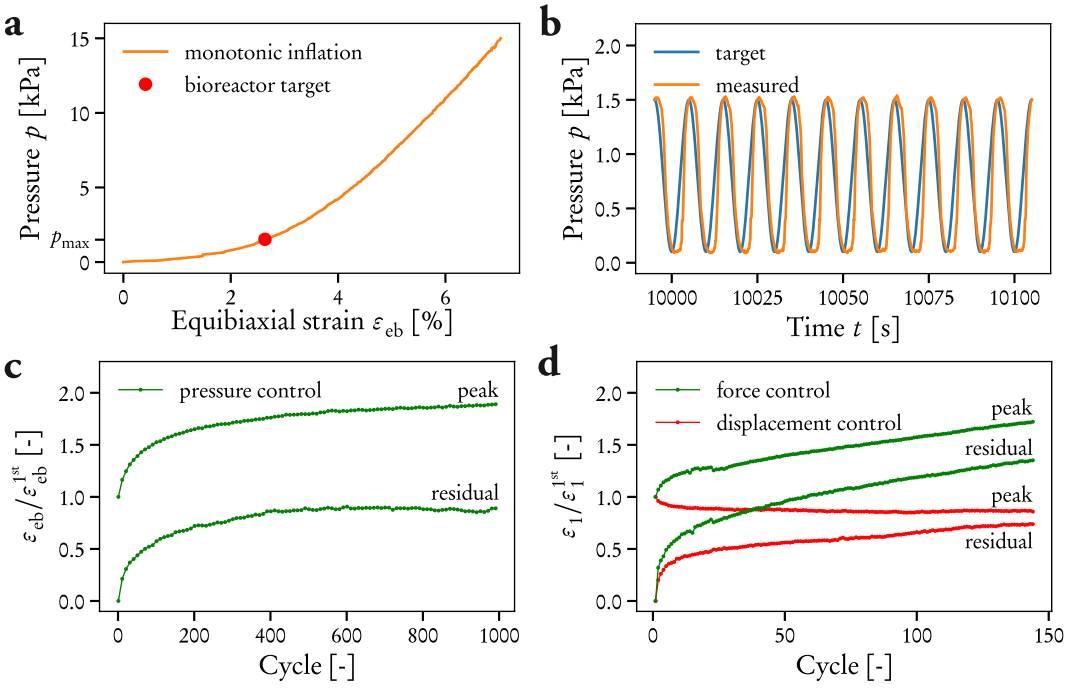

Fig. 3. Mechanical characterization and validation of the dynamic bioreactor system. (**a**) Monotonic pressure-controlled inflation of an acellular dermal substitute; the chosen bioreactor target pressure is indicated with a red dot. (**b**) Excerpt from 11 cycles of a dynamic culturing experiment, demonstrating reliable pressure control. (**c**, **d**) Cyclic behavior of acellular dermal substitutes under pressure-controlled inflation (**c**) and uniaxial tension (**d**), showing the effect of plastic deformation. Both peak and residual strains in **c** and **d** are normalized with respect to the first peak strain, ε_{eb}^{1st} and ε_1^{1st}, respectively. (For interpretation of the references to color in this figure legend, the reader is referred to the Web version of this article.)

(Fig. 3a), a target pressure $p_{max} = 1.5$ kPa that results in moderate in-plane strains (~2.5%) was chosen for subsequent dynamic culturing experiments (Fig. 3a, red dot). The target time history of the inflation pressure can be reliably controlled with the PID feedback loop implemented (Fig. 3b). During cyclic pressure-controlled inflation loading, the peak and residual equibiaxial strains quickly increase until stabilized conditions are reached after ~600 cycles, indicating plastification and ratcheting of the hydrogel (Fig. 3c). This behavior was confirmed in cyclic uniaxial tension tests (Fig. 3d, green curves), in which force-controlled loading similarly shows increasing peak and residual strains and cyclic ratcheting. In contrast, the displacement-controlled protocol naturally limits the peak strains; however, the actual elastic strain imposed during a loading cycle approaches zero as the residual strain increases (Fig. 3d, red curves).

3.2. Tissue and fibroblast response to dynamic culturing

3.2.1. Material and structural properties

The mechanical properties of dynamically cultured dermal substitutes are reported in Fig. 4. Fig. 4a depicts a testpiece from a dynamically cultured hydrogel, with Fig. 4bc showing the local stress–stretch (Fig. 4b, left axis) and tension–stretch (Fig. 4b, right axis) curves and the in-plane kinematics (Fig. 4c) in the sample center. The material stiffness E, membrane stiffness K, and Poisson's ratio ν_{12} were evaluated at $\lambda_1 = 1.05$ (cf. Fig. 4bc) and compared with those of controls kept in static culture for 3 or 7 days, as well as data on human skin [33]. Dynamic culturing leads to a three-fold increase in material stiffness compared to the corresponding static control (Fig. 4d; $P < 0.05$), whereas the membrane stiffness remains unchanged (Fig. 4e; $P = 0.12$). Moreover, the dynamic culturing leads to an increase in the in-plane Poisson's ratio (Fig. 4f; $P < 0.05$) with values of 12.8 ± 1.7 (center) and 11.1 ± 1.2 (rim), even higher than previously reported for collagen hydrogels [52–54]. Finally, despite the heterogeneous strains applied to the hydrogel during the bioreactor treatment, the gel appears to be homogeneous in terms of macroscale mechanical properties (compare center and rim, Fig. 4def).

3.2.2. Dynamic culturing induces rapid fibroblast proliferation

The quantification of cell viability, cell density, and cell number is shown in Fig. 5abc. Fig. 5a reports the analysis of the FdA–PI assay, showing high FB viability in the dynamically treated gels, comparable to the static controls ($P = 0.27$) and thus confirming the sterile operation and non-cytotoxic environment of the developed bioreactor. Moreover, a large increase in cell density is observed (Fig. 5b; $P < 0.05$). However, the cell density is influenced not only by cell proliferation but also by changes in gel thickness (Supplementary Fig. S2). To determine the increase in cell number due to proliferation, the number of cells was counted throughout the whole gel thickness but with equal in-plane area, and the change with respect to the cell count in 3d static was calculated. This number is reported in Fig. 5c, revealing a rapid increase in cell number due to dynamic culturing ($P < 0.05$); after three days, (79 ± 19)% and (74 ± 25)% more cells are present in the center and the rim, respectively, compared to when the gel is kept in static culture.

The large increase in cell number suggests a strong upregulation of cell proliferation at the protein and mRNA levels. Whole-mount stainings for the nuclear proliferation marker Ki67 confirmed the former (Fig. 5defg; $P < 0.05$). The increase in cell number is also clearly visible (Fig. 5d'e'f', merged channels). Furthermore, RT-qPCR analysis of the Ki67 mRNA expression corroborates this result, see Fig. 5h. Note that, in general, the FB proliferation response to dynamic culturing is similar in the center and the rim.

To investigate one biological pathway that might be involved in translating the mechanical and extracellular cues perceived during dynamic culturing to cell proliferation, we performed IF stainings for the transcriptional coactivator YAP (Yes-associated protein 1) [55] (Supplementary Fig. S3). Upon translocation to the nucleus, YAP regulates gene expression and induces cell proliferation (via induction of Ki67) [56]. Indeed, quantification of nuclear YAP in dermal FBs shows a strong activation and nuclear translocation in dynamically cultured gels compared to static controls (Supplementary Fig. S3abc). Whereas only 20% of the cells show nuclear YAP under static conditions, this fraction increases to >60% under dynamic conditions (Supplementary Fig. S3d).

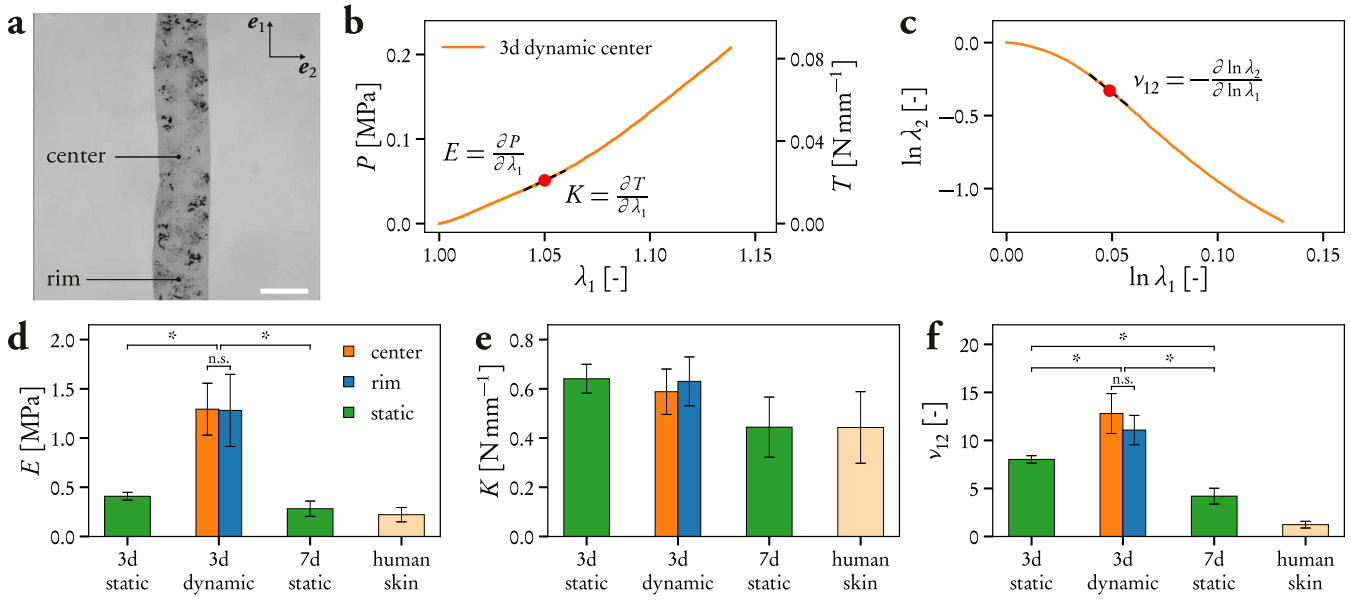

Fig. 4. Mechanical properties of dynamically cultured dermal substitutes. (**a**) Uniaxial tension test of a dynamically cultured sample (scale bar: 5 mm). (**b**, **c**) Representative nominal stress–stretch and tension–stretch curves and in-plane kinematics, obtained from the center of the specimen shown in **a**, together with definitions of the scalar quantities used for group comparisons: (**d**) material stiffness E; (**e**) membrane stiffness K; and (**f**) Poisson's ratio ν_{12}. Significant differences between groups ($P < 0.05$) are indicated with an asterisk; n.s., not significant (one-way ANOVA with Tukey's HSD post-hoc test).

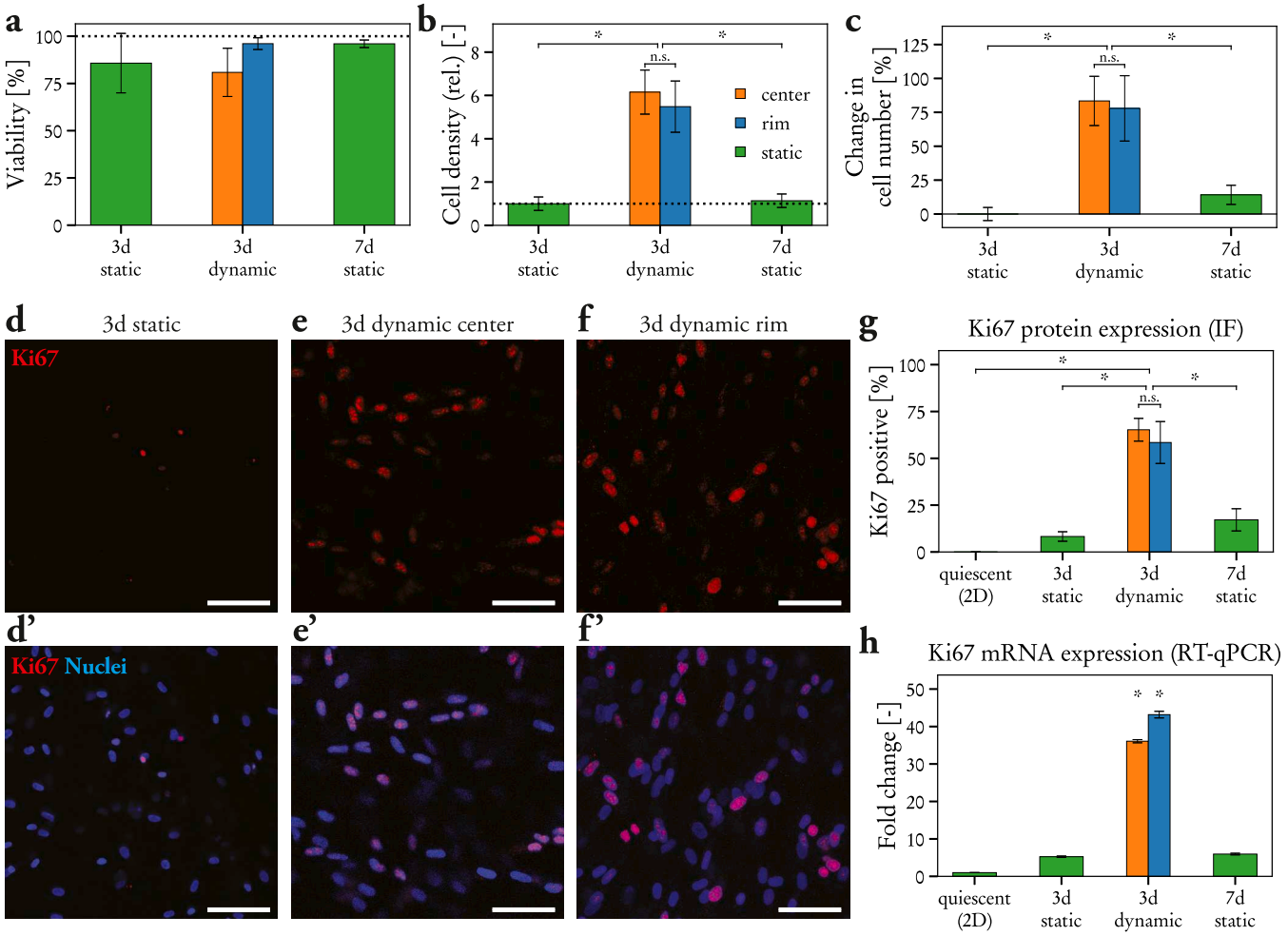

Fig. 5. Fibroblast (FB) viability, density, and proliferation after different culturing protocols. (**a**) FBs remain viable after three days of dynamic culturing. (**b**, **c**) Increase in cell density (**b**) and cell number (**c**) after dynamic culturing. In comparison, note the modest increase in cell number over seven days in static culture. (**d**, **e**, **f**) Whole-mount immunofluorescence (IF) staining for Ki67, a protein expressed in the nucleus and associated with cell proliferation; the quantification of Ki67-positive cells is shown in **g**. The strong upregulation in dynamic culture is present also in the Ki67 mRNA expression (**h**, relative Ki67 gene expression ratio with respect to quiescent FBs in 2D culture). Significant differences ($P < 0.05$) between groups (**b**, **c**, **g**) or with respect to quiescent FBs (**h**) are indicated with an asterisk; n.s., not significant (one-way ANOVA with Tukey's HSD or Dunnett's post hoc test). Scale bars: 100 μm.

3.2.3. The influence of individual biophysical signals on fibroblast proliferation

Cyclic inflation of the dermal substitutes not only imposes strain on the embedded FBs, but also leads to an increase in material stiffness of the surrounding dermal matrix (Fig. 4d) as well as induces interstitial fluid flow through the hydrogel due to the pressure difference between the upper and lower compartments. Importantly, all of these cues might affect FB proliferation [36,37,57]. To investigate the separate roles of these stimuli in inducing FB proliferation, we performed a set of experiments in which one or two of these signals were suppressed (see Supplementary Table S2). The influence of matrix stiffness was analyzed by creating collagen hydrogels of increased collagen concentration, achieved through plastic compression using inserts with prescribed thickness (Fig. 6a). During plastic compression, interstitial fluid trapped within the collagen fiber network is irreversibly forced out of the hydrogel; this results in an increase in the volume fraction of collagen and thus an increase in material stiffness (*cf.* [5,58]). The influence of interstitial fluid flow was analyzed by applying cyclic pressure while hindering the gel from stretching by means of a porous filter and customized clamps (Supplementary Fig. S4a). Additionally, dynamic culturing experiments were performed as previously described (Sec. 2.2) but interrupted after 1.5 days, when gels were either analyzed immediately or placed in free-floating static culture for the remaining 1.5 days.

In statically cultured gels with increasing stiffness, cell number is only moderately correlated with matrix stiffness (Fig. 6c; $r = 0.48$, $P = 0.19$). In particular, a stiffness increase similar to the one obtained after dynamic culturing does not result in the large increase in cell number seen after equal culturing time in the dynamic bioreactor. This result was confirmed on the Ki67 protein level (Fig. 6d). In fact, a strong upregulation is seen already after 1.5 days of dynamic culturing, much higher than with increased stiffness only (Fig. 6d). Interestingly, an upregulation in response to stiffness alone can be clearly detected on the mRNA level (Fig. 6e). Furthermore, the application of cyclic pressure while restricting the gel from stretching did not yield an increase in Ki67 expression (Supplementary Fig. S4). Finally, we note that while both Ki67 protein and mRNA expression are highly upregulated already after 1.5 days of dynamic culturing, the mRNA expression drops rapidly to levels comparable to the static control when the gels were removed from the bioreactor (Fig. 6e). In contrast, protein levels remain high even 1.5 days after the dynamic treatment was stopped (Fig. 6d). This suggests that the upregulation of FB proliferation is reversible and FBs do not remain in a hyperproliferative state.

3.2.4. Fibroblast stress fiber orientation in response to dynamic culturing

Representative confocal micrographs of the immunostained F-actin

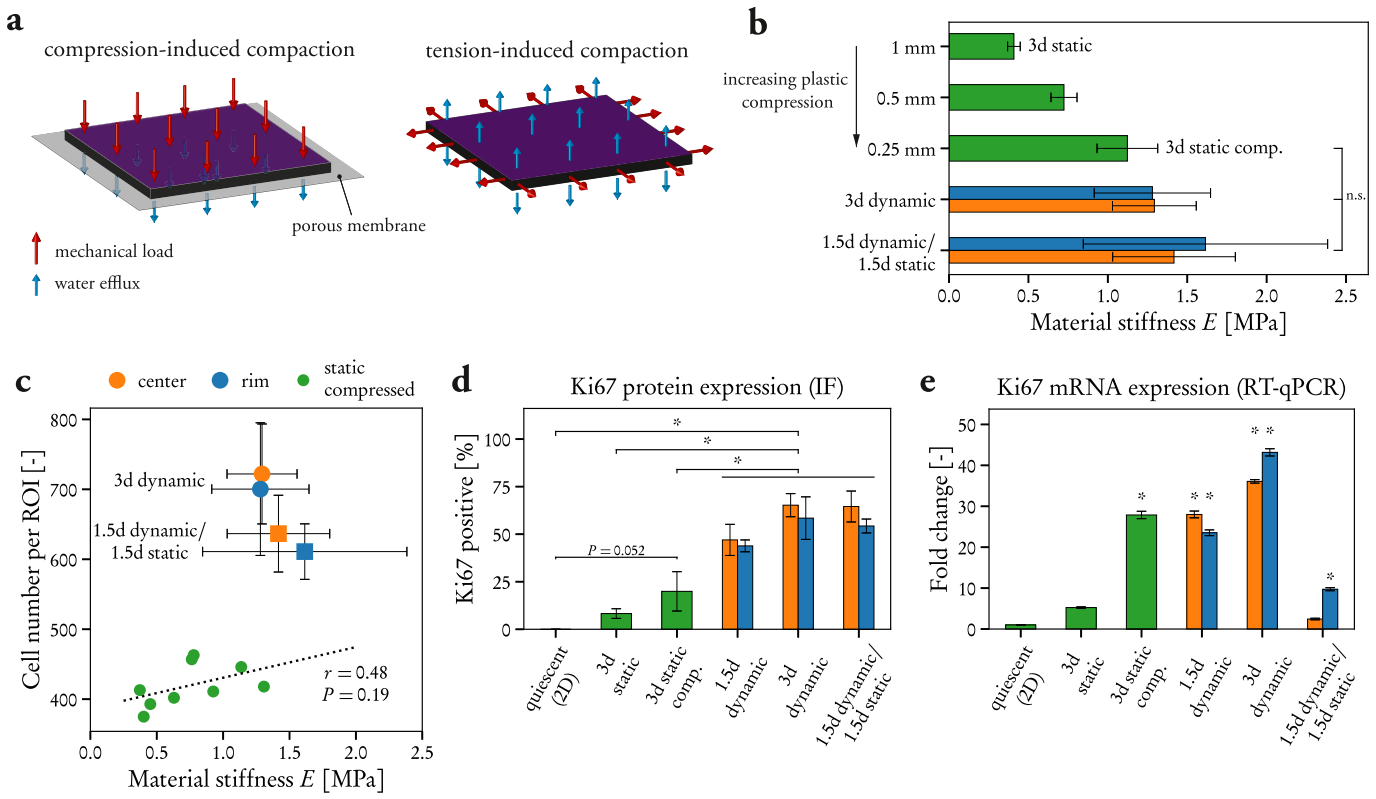

Fig. 6. The separate effects of matrix stiffness and cyclic loading on fibroblast proliferation. (**a**) Plastic compression results in irreversible water efflux and hydrogel compaction similarly as when gels are exposed to in-plane tension. (**b**) Reducing gel thickness by plastic compression allows replicating the stiffness of dynamically cultured hydrogels ($P = 0.73$, one-way ANOVA). (**c**) Correlation between cell number and hydrogel stiffness ($r = 0.48$, $P = 0.19$, Pearson's correlation test) can not explain the rapid proliferation in dynamic culture. (**d**, **e**) Ki67 expression on the protein level (**d**) and mRNA level (**e**), showing the temporal evolution of the proliferation response in static and dynamic culture and the effect of increasing matrix stiffness. Significant differences between groups (**d**) or with respect to quiescent FBs (**e**) are indicated with an asterisk (one-way ANOVA with Tukey's HSD or Dunnett's post-hoc test). In **b**–**e**: orange—dynamic center; blue—dynamic rim; green—static compressed. (For interpretation of the references to color in this figure legend, the reader is referred to the Web version of this article.)

of FBs after three days of static *vs.* dynamic culture are shown in Fig. 7. Whereas FBs in static controls (Fig. 7a) as well as in the center of dynamically cultured gels (Fig. 7b) locally tend to have only a slight preference in direction, FBs in the rim uniformly orient in the circumferential direction, *i.e.* perpendicular to the maximum principal strain direction (Fig. 7c). The difference in FB alignment was quantified in terms of the probability density of the F-actin orientation, incorporating information from all biological replicates (Fig. 7d). This indicates that cells clearly distinguish between the different regions of the dynamically cultured gels.

Since mechanical tension [59] and increased substrate stiffness [35] are known to stimulate FB differentiation into highly contractile myofibroblasts [60], which in turn may cause contraction and formation of scar-like tissue, we further assessed whether α-smooth muscle actin (α-SMA) was incorporated into the stress fibers of FBs in static and dynamic culture. Representative confocal micrographs (Fig. 7fgh) show that only few cells display α-SMA-positive stress fibers; importantly, this is observed both in statically (Fig. 7f) and dynamically cultured gels (Fig. 7gh).

3.3. Keratinocyte growth on dynamically cultured dermal substitutes

The analysis of KC viability, surface coverage, and proliferation three days after seeding on top of dermal matrices is shown in Fig. 8. Prior to KC seeding, the dermal matrices were preconditioned by FBs for three or seven days in static conditions (controls) or for three days in dynamic culture. The dermal matrices with KCs were thereafter cultured for three days in static conditions (cf. Fig. 2 and Table 1). When KCs are cultured on top of statically preconditioned matrices, KC coverage remains incomplete (Fig. 8ac). In contrast, KCs on top of dynamically cultured matrices are able to form a monolayer and completely cover the surface within three days (Fig. 8b). By segmenting the images (see Supplementary Fig. S5), the coverage was quantified (Fig. 8d), demonstrating the consistent KC coverage on dynamically cultured dermal substitutes (>99% for all three experiments) compared to (83.67 ± 11.17)% and (85.48 ± 3.05)% when seeded on top of dermal matrices preconditioned by FBs in static culture for three and seven days, respectively. Whole-mount immunostaining for Ki67 shows a higher KC proliferation rate on dynamically cultured dermal matrices compared to on static controls (Fig. 8e–h), suggesting that the complete surface coverage reached by KCs is due to the higher proliferation rate supported by the dynamically cultured dermal substitutes.

3.4. Dynamic culturing improves early maturation of human skin substitutes

To analyze whether dynamic culturing can accelerate the early maturation of the dermo–epidermal skin substitutes, we analyzed a set of established markers indicative of dermo–epidermal skin substitute homeostasis [10]. Representative IF images are shown in Fig. 9a–h. KCs were stained for their specific marker pan-cytokeratin (PanCK) and analyzed in parallel for the expression of E-cadherin, a component of the adherens junctions (Fig. 9a). We confirmed that after three days in culture, KCs seeded on statically cultured hydrogels form an incomplete monolayer (Fig. 9ab, arrows), which is lacking the expression of E-cadherin. In contrast, the epidermis formed on the dynamically cultured dermal substitutes appears like a continuous monolayer, strongly expressing E-cadherin (Fig. 9a). These results are also

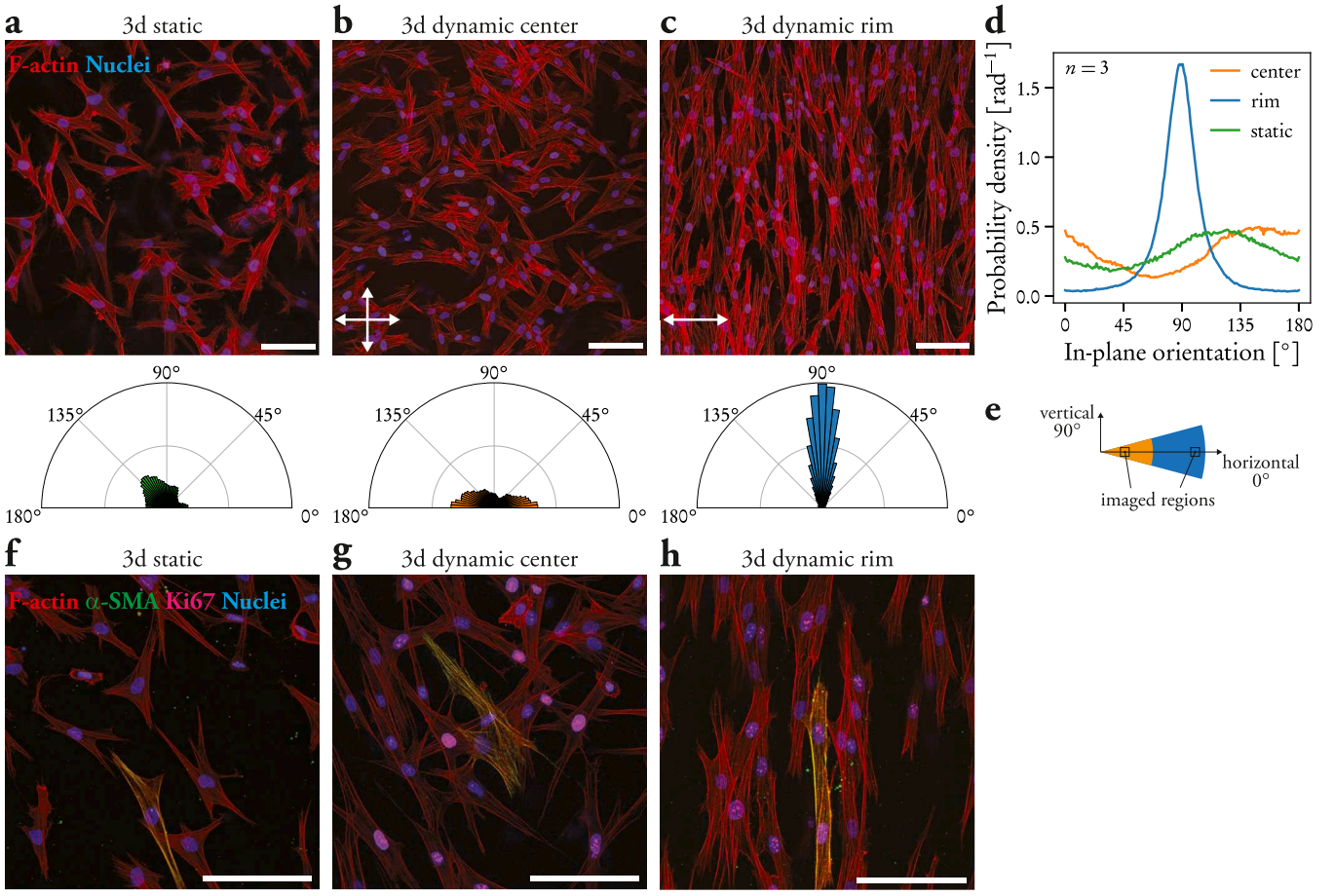

Fig. 7. Fibroblast stress fiber reorientation in response to cyclic loading. Representative confocal micrographs of phalloidin-stained F-actin after three days of static (**a**) or dynamic culture (center: **b**; rim: **c**) together with corresponding polar histograms of the F-actin fiber orientation. The image orientation with respect to the gel locations imaged is schematically depicted in **e**. (**d**) The estimated probability density of F-actin orientation per condition and region, averaged over $n = 3$ biological replicates. The in-plane main strain directions during dynamic culturing are indicated in **b** and **c** with white arrows. (**f**, **g**, **h**) Representative micrographs of fibroblasts stained for F-actin, α-SMA, and Ki67, showing scant presence of α-SMA-positive myofibroblasts in all conditions. Scale bars: 100 μm.

supported by whole-mount stainings for E-cadherin expression in the epidermis (Fig. 9b). In addition, KCs cultured on statically preconditioned matrices show low expression of CK15 and CK19 (Fig. 9c), two markers indicative of a mature basal layer and epidermal homeostasis. These markers are instead strongly expressed when KCs are cultured on matrices that previously underwent dynamic treatment (Fig. 9c). Corresponding whole-mount stainings for CK19 confirm these results (Fig. 9d). To check for the presence of dermo–epidermal junctions, we stained for integrin β4 and α6, components of the hemidesmosomes that mediate KC anchorage to the basal lamina. Whereas in the static control both β4 and α6 are missing, they are continuously expressed in all KCs seeded on dynamically preconditioned hydrogels (Fig. 9ef).

The maturation of the dermo–epidermal skin substitutes was further analyzed through the expression of two major dermal ECM components, collagen type I and the precursor of elastic fibers, tropoelastin (Fig. 9gh). The collagen fiber network appears denser and aligned parallel to the epidermis in the dynamically treated dermal substitutes (Fig. 9g, arrows). Tropoelastin is almost undetectable in the static controls (Fig. 9h), whereas an extensive and dense network exists throughout the dermis in the dynamically treated hydrogels (Fig. 9h, asterisks). Co-staining with Ki67 confirms the higher proliferation rate of both KCs and FBs in the dynamically treated dermal substitutes (Fig. 9gh). The individual channels of each staining are reported in Supplementary Figs. S7–S9.

RT-qPCR analysis of the dermal part revealed a general upregulation of markers indicating early maturation of the skin. Collagen I (COL1A1) is upregulated 7.5-fold and 17.5-fold in the center and rim, respectively, compared to the static control (Fig. 9i). A similar effect can be observed for elastin (ELN), with a 12- and 20-fold upregulation for center and rim, respectively (Fig. 9k). Elastin confers crucial elastic properties to the skin and allows the skin to resume its shape after stretching. The dynamic culturing induces an increase in the expression of collagen IV (COL4A1) and fibronectin (FN1), although not statistically significant compared to static controls (Fig. 9jl). Collagen IV is important for the development of the basal lamina, and fibronectin is a glycoprotein that binds to collagen and serves as an important integrin-binding partner within the ECM. The analysis also suggests an upregulation of tissue transglutaminase (TG2) on the mRNA level in the dynamically cultured gels (Fig. 9m).

4. Discussion

Tissue engineering of autologous skin grafts that can provide permanent wound coverage and promote healing with minimal scarring is an innovative approach to the treatment of large, full-thickness wounds. However, the production time of clinically applicable skin grafts remains on the order of one month, which may limit their application. Here, we show the proof of principle that our novel bioreactor and dynamic culturing method, which induces rapid FB proliferation in a physiologically relevant, three-dimensional dermal matrix that further supports faster establishment of an early epidermis, can speed up the early tissue maturation. Our results indicate that a comparable tissue

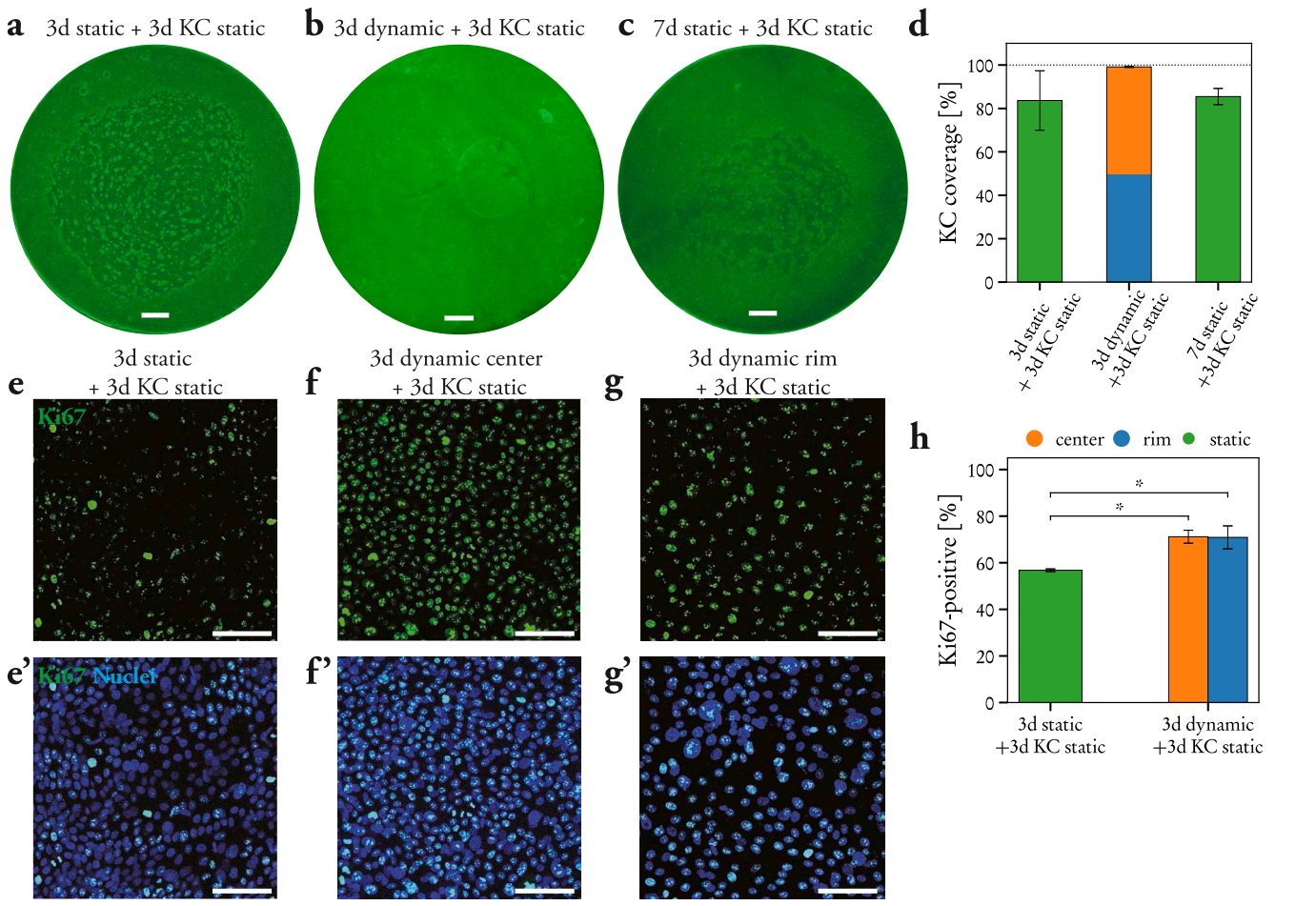

Fig. 8. Keratinocyte (KC) viability, coverage, and proliferation on dynamically treated dermal substitutes. (**a**, **b**, **c**) Representative fluorescence images of FdA-stained KCs on top of dermal matrices precultured for three (**a**) or seven days statically (**c**) or three days in the dynamic bioreactor (**b**). Scale bars (**a**–**c**): 2 mm. Images were acquired three days after KC seeding. The images were segmented and the percentage area covered by KCs was quantified for the three conditions (**d**; $P = 0.11$, one-way ANOVA). (**e**, **f**, **g**) Whole-mount immunofluorescence staining for Ki67 shows higher KC proliferation on dynamically preconditioned dermal matrices. The quantification of Ki67-positive KCs is shown in **h** ($P < 0.05$, one-way ANOVA with Tukey's HSD post-hoc test). Scale bars (**e**–**g**): 100 μm.

can be formed in one week instead of the two weeks required under static conditions, which suggests a potential 1 week reduction in the overall production time of four to five weeks under static conditions. The design, use, and evaluation of such bioreactor systems for skin tissue engineering requires consideration of several technical and (mechano) biological aspects.

4.1. *Bioreactor design considerations for tissue engineering*

The design of bioreactors for tissue engineering involves several parameters, such as the type of loading (uniaxial, biaxial, and/or shear stresses), load control (displacement or force), as well as the loading frequency, amplitude, and duration, all of which need to be selected based on the target tissue and the specific graft material. As many native biomaterials, including collagen hydrogels (Fig. 3cd) and human skin [33], exhibit some degree of plastic deformation under cyclic loading, this selection requires an important compromise: Most existing bioreactor systems operate in a displacement-controlled manner (either directly [25,27,30] or by actuation of elastic load-bearing elements [22–24]), which, although intrinsically safe, can lead to almost zero mechanical load being applied to the tissue (*cf.* Fig. 3d, red curves). In contrast, force- or pressure-controlled operation as applied here ensures that the tissue is consistently loaded and thus increases the effectiveness (Fig. 3cd); however, the load magnitude has to be chosen such that cyclic ratcheting is limited and does not cause material failure.

The effect of applied cyclic and static strain on tissue-engineered skin and dermal substitutes under uniaxial stress conditions has been investigated previously [29,30]. However, considering that the native skin is exposed to a biaxial rather than uniaxial state of stress *in vivo*, we opted for a membrane inflation-based setup where the tissue is exposed to biaxial, albeit heterogeneous stresses. Importantly, this avoids inducing strong fiber alignment and corresponding anisotropy of the graft material, and better replicates the more random fiber network structure of the dermis.

4.2. *Dermal matrix remodeling is driven by network deformations*

The remodeling of the dermal matrix observed during dynamic culturing, consisting of a three-fold increase in material stiffness E (Fig. 4d) and an increased in-plane Poisson's ratio ν_{12} (Fig. 4f), while the membrane stiffness K remained unchanged (Fig. 4e), calls for the question whether the remodeling is due to deformation-driven rearrangements of the matrix or a result of cell activities. In fact, the constant K suggests that, macroscopically, the quantity and organization of collagen fibers are conserved and that cell remodeling of the ECM plays a minor role. To test this interpretation of minimal effect of cell-induced remodeling, we exposed an acellular hydrogel to the same dynamic culturing protocol and analyzed its resulting properties; indeed, the nominal tension and in-plane kinematics are very similar to those of the dynamically cultured cellular gels (Supplementary Fig. S6ab).

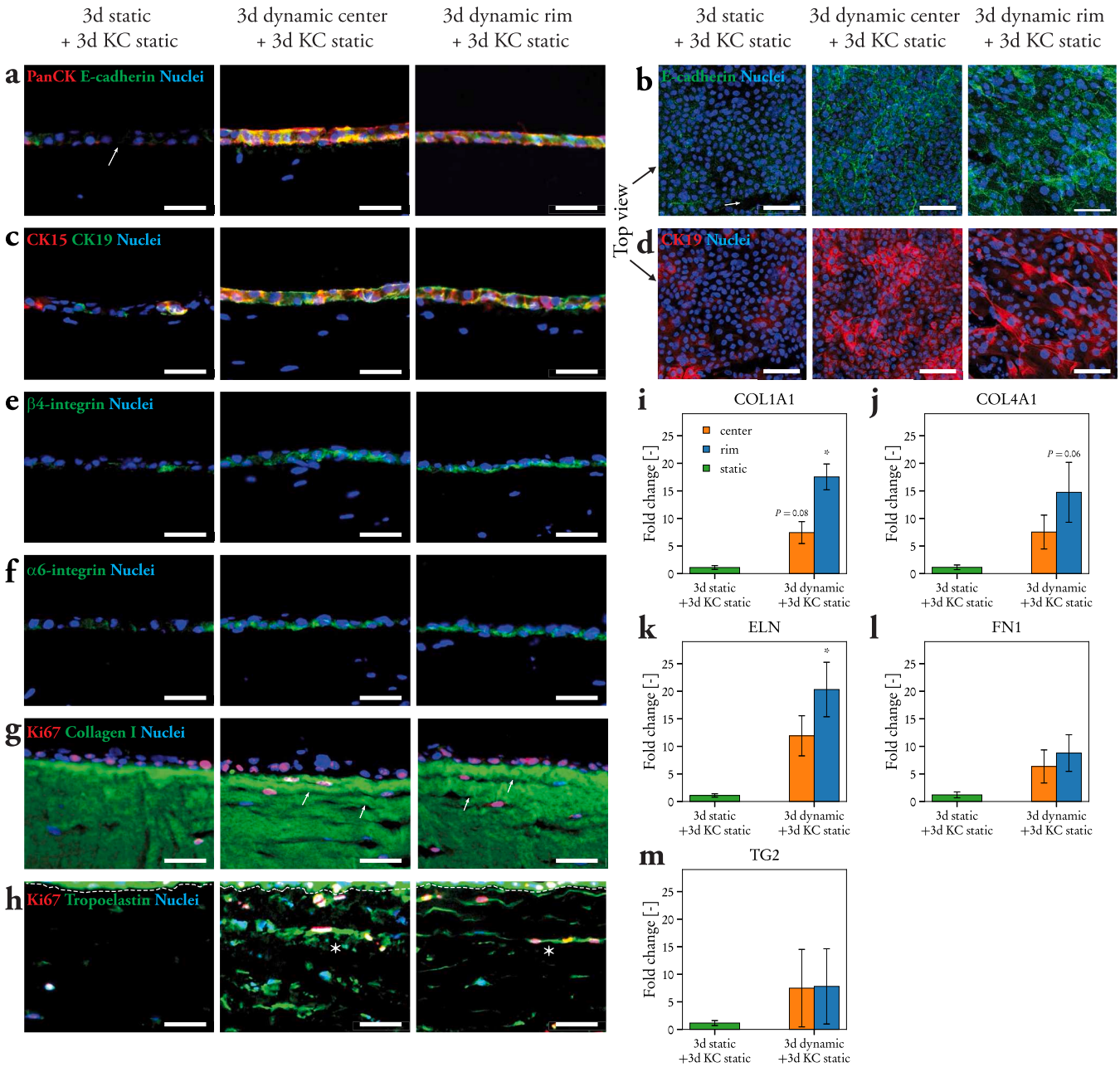

Fig. 9. Dynamic culturing improves early maturation of human skin substitutes. (**a**–**h**) Representative immunofluorescence micrographs of dermo–epidermal skin substitutes that were precultured statically or dynamically for three days, seeded with keratinocytes (KCs), and further cultured statically for an additional three days. Dynamic preculturing stimulates the development of a continuous monolayer of KCs positive for pan cytokeratin (PanCK) (**a**), E-cadherin (**a**, **b**), CK15 (**c**), CK19 (**c**, **d**), β4-integrin (**e**), and α6-integrin (**f**) in contrast to static preculturing. A denser and more aligned collagen I matrix can be observed after dynamic culturing (**g**, arrows). In addition, staining for Ki67 confirms the higher proliferation rate of both KCs and FBs due to dynamic preculturing (**g**, **h**). Tropoelastin (**h**, asterisks) is strongly expressed in the dermis of dynamically precultured skin substitutes. (**i**–**m**) RT-qPCR analysis of dermis-related ECM markers shows a general upregulation of genes in both center and rim of dynamically treated gels compared to static controls. Significant upregulation was observed for COL1A1 (rim, **i**) and for ELN (rim, **k**) ($P < 0.05$, one-way ANOVA with Dunnett's post-hoc test). White dashed line: dermo–epidermal border. Scale bars (**a**, **c**, **e**–**h**): 50 μm. Scale bars (**b**, **d**): 100 μm.

Additionally, we note that a similar progression in mechanical properties is observed by solely increasing the level of plastic compression (Fig. 6ab and Supplementary Fig. S6cde). These results are in agreement with our previous work, where no differences between acellular and FB-containing plastically compressed collagen hydrogels were observed even after five days in static culture [52].

In contrast, other studies have reported a significant cell-induced increase in the stiffness of tissue-engineered grafts when undergoing dynamic culturing (*e.g.* [22,25,27,28,30]). While this result may be expected after several weeks of culture [22,25,27], or may be the combined result of biophysical cues and added biochemical components (*e.g.* ascorbic acid, transforming growth factor β1) known to stimulate ECM deposition by cells [28,30], a proper comparison is difficult since most studies only report changes in *material* stiffness and strength. It is therefore important to also consider the properties of the tissue-engineered graft as a mechanical *structure*—not only to determine whether remodeling is mediated by cells or by purely physical mechanisms, but also to evaluate the load-bearing function of the graft.

4.3. Cyclic strain and material stiffness determine fibroblast proliferation

When cultured within dilute collagen gels, FBs are quiescent and can only start to divide once the matrix can provide sufficient resistance to the cells' traction forces [36,61]. With plastic compression [58], a dense collagen matrix can be created, which provides an optimal ECM [5] that has mechanical properties resembling those of the human skin (Fig. 4). However, in this matrix the rate of FB proliferation is still low (Fig. 5), with only a (14 ± 7)% increase in cell number from day 3 to day 7 in static culture. In contrast, FBs were observed to quickly re-enter the cell cycle and to start dividing when cultured under dynamic conditions (Fig. 5). An upregulation of cell proliferation has been reported for various cell types when cultured on top of flexible elastic substrates (*e.g.* [57,62–65]) and in three-dimensional constructs [66,67] that undergo cyclic strain. In a similar native collagen type I matrix, Hadjipanayi et al. [36] found a strong correlation between FB proliferation and increased matrix stiffness. Our experiments reported in Fig. 6 confirm the role of matrix stiffness in stimulating cell cycle entry, and furthermore show that the cell response to the stiffness of their highly heterogeneous native ECM is considerably slower compared to their response to the mechanical cues imparted by cyclic stretching. Together with the negligible effect of interstitial fluid flow on FB proliferation (Supplementary Fig. S4), we therefore conclude that cyclic strain is the main biophysical factor inducing FB proliferation.

4.4. Heterogeneity and homogeneity of the dermal matrix

Membrane inflation leads to a biaxial state of stress, from close to equibiaxial in the center of the inflated hydrogel to strip biaxial (uniaxial strain) close to the clamping (Fig. 2g). Cells do perceive the regional differences, as demonstrated by their striking reorientation behavior in the rim region (*cf.* Fig. 7bc). We note that FBs in the rim reorient in the circumferential direction, perpendicular to the applied radial strain, which is similar to cells on 2D substrates exposed to cyclic strain that reorient to minimize their elastic strain energy [68]. In contrast, cells embedded in 3D gels undergoing static or slow cyclic loading have been reported to align in the direction of applied stress [30,69,70], and reorient similarly as observed in 2D only at frequencies above 2 Hz [70]. The differences in reorientation behavior between 2D and 3D environments have been proposed to depend on the contact guidance provided by the fibrillar environment [71], which in our case would predict radial rather than circumferential FB alignment. A better explanation for the circumferential cell and stress fiber orientation is the higher stiffness sensed due to the boundary constraint in the rim region [72], which is also in agreement with the preferential cell alignment in the stiffest direction observed on top of arrays of anisotropic micropillars [73].

It is therefore surprising that despite the stress and strain heterogeneity between the center and the rim, the mechanical properties (Fig. 4def), FB proliferation (Fig. 5), as well as KC coverage (Fig. 8b), proliferation (Fig. 8fgh), and early epidermis maturation (Fig. 9a–h) are unaffected. This indicates that FB orientation and differences in collagen network microstructure between center and rim do not result in significant differences in material properties and cell behavior—an important finding for skin tissue engineering applications.

4.5. Improved epidermal growth on dynamically cultured dermal matrices

It is generally understood that the *in vitro* proliferation of KCs depends on interactions with dermal FBs [74]. This has also been demonstrated in the context of dermo–epidermal skin substitutes, where KCs grow poorly on top of acellular collagen type I hydrogels [75]. In our statically cultured skin substitutes, a minimum time for FBs to precondition the matrix of around one week is required for successful KC migration, proliferation, and stratification [15]. Here, we demonstrate that dynamic preculturing of the dermal matrix results in reorganization of the collagen network, increased secretion of elastic proteins, and an upregulation of several ECM markers on the transcriptional level (Fig. 9). This further stimulates KC expression of adhesive proteins (β4-integrin, α6-integrin), E-cadherin, CK15, and CK19 (Fig. 9), which are crucial for the early establishment of the epidermis [10,76–78]. Another contributing factor to the increased KC proliferation might be the increased rigidity of the dermal matrix [79,80].

Note that in our experiments, KCs were not exposed to cyclic loading. It was recently shown that static stretching in an *in vivo* skin expander model induces proliferation in a subpopulation of basal KCs [81]. Exposing also the KCs to cyclic loading may therefore further increase proliferation and accelerate the early maturation of the epidermis.

4.6. Relevance for skin tissue engineering

Compared to our optimized static culturing protocols [14,15], the dynamic bioreactor and cultivation method described here offers a potential 1 week reduction in *in vitro* culturing time of our human dermo–epidermal skin substitutes. Clearly, the efficacy of dynamic culturing needs to be further assessed in an *in vivo* setting. In view of this, improved wound healing in terms of reduced myofibroblast persistence and, consequently, reduced scar contraction, has been reported when treating wounds with dermal matrices containing higher number of autologous FBs [82]. Importantly, our dynamic culturing protocol yields a strong increase in the number of FBs without inducing activation of α-SMA-positive myofibroblasts (Fig. 7f–h), despite the three-fold increase in matrix stiffness (Fig. 4d). Although studies on FBs in 2D culture have shown that matrix stiffening can induce spontaneous myofibroblast differentiation [35], our results are in line with the general inverse relationship expected between cell proliferation and differentiation [83]. Taken together, the higher number of FBs and the higher material stiffness suggest that the dynamically cultured dermo–epidermal skin substitutes may undergo less contraction upon transplantation, which is of clinical importance in minimizing scar formation [12].

Our future work will focus on the analysis of dermal–epidermal interactions during cyclic loading, upscaling and development of a parallelized bioreactor setup, and the preclinical *in vivo* application of dynamically cultured skin substitutes in an animal model.

5. Conclusions

We developed a novel dynamic bioreactor system to investigate whether applying cyclic biaxial tension to bioengineered human skin equivalents can accelerate the early tissue maturation and thus reduce the total production time. The results show that cyclic deformation leads to a stiffening of the dermal matrix and stimulates rapid fibroblast proliferation, but does not affect fibroblast differentiation into myofibroblasts. Tissue maturation is therefore enhanced, as demonstrated by the increased expression of dermal extracellular proteins and markers of epidermal homeostasis. This results in a significantly shorter culturing time compared to under static conditions. Regional differences in the mechanical signals affect fibroblast orientation but neither fibroblast proliferation, early epidermis formation, nor the mechanical properties of the tissue. Proper control of mechanobiological cues therefore holds great potential in guiding cell behavior toward a faster graft development and eventually an improved outcome for patients suffering from severe skin defects.

Declaration of competing interest

The authors declare the following financial interests/personal relationships which may be considered as potential competing interests: E. R. is a founding member of CUTISS AG, a biotech start-up developing the here-described cultured autologous dermo-epidermal skin substitute toward manufacturing scale-up and commercialization. The other authors declare that they have no competing interests.

Acknowledgments

This work was conducted as part of the Skintegrity project of University Medicine Zurich and was financially supported by the Swiss National Science Foundation (grant no. 179012). We would like to thank Jean–Claude Tomasina, Bernhard Zybach, and Jung–Chew Tse for manufacturing support and Matilde Fiori for her contributions to the bioreactor design.

Appendix A. Supplementary data

Supplementary data to this article can be found online at https://doi.org/10.1016/j.biomaterials.2021.120779.

Author contributions

A.W., D.R., T.B., E.R., and E.M. designed the study. E.M. and A.W. conceptualized the dynamic bioreactor for skin tissue engineering; A.W. designed and characterized the bioreactor and developed the dynamic culturing protocol. D.R., A.W., M.N., and C.G. performed the experiments. A.W., D.R., and M.N. analyzed the data and prepared the figures, and A.W. and D.R. wrote the manuscript. E.M., E.R., and T.B. supervised the study, reviewed and edited the manuscript, and acquired the funding. All authors discussed the results and reviewed the manuscript.

Data availability

The data that support the findings are available from the corresponding authors upon reasonable request.

References

[1] S. MacNeil, Progress and opportunities for tissue-engineered skin, Nature 445 (7130) (2007) 874–880, https://doi.org/10.1038/nature05664.
[2] S. Böttcher–Haberzeth, T. Biedermann, E. Reichmann, Tissue engineering of skin, Burns 36 (2010) 450–460, https://doi.org/10.1016/B978-0-12-381422-7.10057-4.
[3] A.L. Rippa, E.P. Kalabusheva, E.A. Vorotelyak, Regeneration of dermis: scarring and cells involved, Cells 8 (6) (2019) 607, https://doi.org/10.3390/cells8060607.
[4] E. Bell, H.P. Ehrlich, D.J. Buttle, T. Nakatsuji, Living tissue formed in vitro and accepted as skin-equivalent tissue of full thickness, Science 211 (4486) (1981) 1052–1054.
[5] E. Braziulis, M. Diezi, T. Biedermann, L. Pontiggia, M. Schmucki, F. Hartmann–Fritsch, J. Luginbühl, C. Schiestl, M. Meuli, E. Reichmann, Modified plastic compression of collagen hydrogels provides an ideal matrix for clinically applicable skin substitutes, Tissue Eng. C Methods 18 (6) (2012) 464–474, https://doi.org/10.1089/ten.tec.2011.0561.
[6] J.F. Hansbrough, S.T. Boyce, M.L. Cooper, T.J. Foreman, Burn wound closure with cultured autologous keratinocytes and fibroblasts attached to a collagen-glycosaminoglycan substrate, J. Am. Med. Assoc. 262 (15) (1989) 2125–2130, https://doi.org/10.1001/jama.1989.03430150093032.
[7] M. Michel, N. Uheureux, R. Pouliot, W. Xu, F.A. Auger, L. Germain, Characterization of a new tissue-engineered human skin equivalent with hair, Vitr. Cell. Dev. Biol.-Animal 35 (1999) 318–326.
[8] W. Lee, J.C. Debasitis, V.K. Lee, J.-H. Lee, K. Fischer, K. Edminster, J.-K. Park, S.-S. Yoo, Multi-layered culture of human skin fibroblasts and keratinocytes through three-dimensional freeform fabrication, Biomaterials 30 (8) (2009) 1587–1595, https://doi.org/10.1016/j.biomaterials.2008.12.009.
[9] S.T. Boyce, R.J. Kagan, K.P. Yakuboff, N.A. Meyer, M.T. Rieman, D.G. Greenhalgh, G.D. Warden, S. Boyce, Cultured skin substitutes reduce donor skin harvesting for closure of excised, full-thickness burns, Ann. Surg. 235 (2) (2002) 269–279.
[10] L. Pontiggia, T. Biedermann, M. Meuli, D. Widmer, S. Böttcher–Haberzeth, C. Schiestl, J. Schneider, E. Braziulis, I. Montaño, C. Meuli-Simmen, E. Reichmann, Markers to evaluate the quality and self-renewing potential of engineered human skin substitutes in vitro and after transplantation, J. Invest. Dermatol. 129 (2) (2009) 480–490, https://doi.org/10.1038/jid.2008.254.
[11] F. Hartmann-Fritsch, T. Biedermann, E. Braziulis, M. Meuli, E. Reichmann, A new model for preclinical testing of dermal substitutes for human skin reconstruction, Pediatr. Surg. Int. 29 (5) (2013) 479–488, https://doi.org/10.1007/s00383-013-3267-y.
[12] A.S. Klar, S. Güven, T. Biedermann, J. Luginbühl, S. Böttcher-Haberzeth, C. Meuli-Simmen, M. Meuli, I. Martin, A. Scherberich, E. Reichmann, Tissue-engineered dermo-epidermal skin grafts prevascularized with adipose-derived cells, Biomaterials 35 (19) (2014) 5065–5078, https://doi.org/10.1016/j.biomaterials.2014.02.049.
[13] D. Marino, J. Luginbühl, S. Scola, M. Meuli, E. Reichmann, Bioengineering dermo-epidermal skin grafts with blood and lymphatic capillaries, Sci. Transl. Med. 6 (221) (2014) 221ra14, https://doi.org/10.1126/scitranslmed.3006894.
[14] M. Meuli, F. Hartmann-Fritsch, M. Hüging, D. Marino, M. Saglini, S. Hynes, K. Neuhaus, E. Manuel, E. Middelkoop, E. Reichmann, C. Schiestl, A cultured autologous dermo-epidermal skin substitute for full-thickness skin defects: a phase I, open, prospective clinical trial in children, Plast. Reconstr. Surg. 144 (1) (2019) 188–198, https://doi.org/10.1097/PRS.0000000000005746.
[15] L. Pontiggia, A. Klar, S. Böttcher-Haberzeth, T. Biedermann, M. Meuli, E. Reichmann, Optimizing in vitro culture conditions leads to a significantly shorter production time of human dermo-epidermal skin substitutes, Pediatr. Surg. Int. 29 (3) (2013) 249–256, https://doi.org/10.1007/s00383-013-3268-x.
[16] S.T. Boyce, P.S. Simpson, M.T. Rieman, P.M. Warner, K.P. Yakuboff, J.K. Bailey, J. K. Nelson, L.A. Fowler, R.J. Kagan, Randomized, paired-site comparison of autologous engineered skin substitutes and split-thickness skin graft for closure of extensive, full-thickness burns, J. Burn Care Res. 38 (2) (2017) 61–70, https://doi.org/10.1097/BCR.0000000000000401.
[17] L. Germain, D. Larouche, B. Nedelec, I. Perreault, L. Duranceau, P. Bortoluzzi, C. B. Cloutier, H. Genest, L. Caouette-Laberge, A. Dumas, A. Bussière, E. Boghossian, J. Kanevsky, Y. Leclerc, J. Lee, M.T. Nguyen, V. Bernier, B.M. Knoppers, V. J. Moulin, F.A. Auger, Autologous bilayered self-assembled skin substitutes (SASSs) as permanent grafts: a case series of 14 severely burned patients indicating clinical effectiveness, Eur. Cell. Mater. 36 (2018) 128–141, https://doi.org/10.22203/eCM.v036a10.
[18] I. Martin, D. Wendt, M. Heberer, The role of bioreactors in tissue engineering, Trends Biotechnol. 22 (2) (2004) 80–86, https://doi.org/10.1016/j.tibtech.2003.12.001.
[19] B.D. Riehl, J.-H. Park, I.K. Kwon, J.Y. Lim, Mechanical stretching for tissue engineering: two-dimensional and three-dimensional constructs, Tissue Eng. B Rev. 18 (4) (2012) 288–300, https://doi.org/10.1089/ten.teb.2011.0465.
[20] J.D. Humphrey, E.R. Dufresne, M.A. Schwartz, Mechanotransduction and extracellular matrix homeostasis, Nat. Rev. Mol. Cell Biol. 15 (12) (2014) 802–812, https://doi.org/10.1038/nrm3896.
[21] J.H. Wang, B.P. Thampatty, An introductory review of cell mechanobiology, Biomech. Model. Mechanobiol. 5 (1) (2006) 1–16, https://doi.org/10.1007/s10237-005-0012-z.
[22] L.E. Niklason, J. Gao, W.M. Abbott, K.K. Hirschi, S. Houser, R. Marini, R. Langer, Functional arteries grown in vitro, Science 284 (5413) (1999) 489–493.
[23] D. Seliktar, R.A. Black, R.P. Vito, R.M. Nerem, Dynamic mechanical conditioning of collagen-gel blood vessel constructs induces remodeling in vitro, Ann. Biomed. Eng. 28 (4) (2000) 351–362, https://doi.org/10.1114/1.275.
[24] E.E. van Haaften, T.B. Wissing, M.C.M. Rutten, J.A. Bulsink, K. Gashi, M.A.J. van Kelle, A.I.P.M. Smits, C.V.C. Bouten, N.A. Kurniawan, Decoupling the effect of shear stress and stretch on tissue growth and remodeling in a vascular graft, Tissue Eng. C Methods 24 (7) (2018) 418–429, https://doi.org/10.1089/ten.tec.2018.0104.
[25] B.-S. Kim, J. Nikolovski, J. Bonadio, D.J. Mooney, Cyclic mechanical strain regulates the development of engineered smooth muscle tissue, Nat. Biotechnol. 17 (10) (1999) 979–983, https://doi.org/10.1038/13671.
[26] D.L. Butler, N. Juncosa-Melvin, G.P. Boivin, M.T. Galloway, J.T. Shearn, C. Gooch, H. Awad, Functional tissue engineering for tendon repair: a multidisciplinary strategy using mesenchymal stem cells, bioscaffolds, and mechanical stimulation, J. Orthop. Res. 26 (1) (2008) 1–9, https://doi.org/10.1002/jor.20456.
[27] R.L. Mauck, M.A. Soltz, C.C. Wang, D.D. Wong, P.H.G. Chao, W.B. Valhmu, C. T. Hung, G.A. Ateshian, Functional tissue engineering of articular cartilage through dynamic loading of chondrocyte-seeded agarose gels, J. Biomech. Eng. 122 (3) (2000) 252–260, https://doi.org/10.1115/1.429656.
[28] J.K. Lee, L.W. Huwe, N. Paschos, A. Aryaei, C.A. Gegg, J.C. Hu, K.A. Athanasiou, Tension stimulation drives tissue formation in scaffold-free systems, Nat. Mater. 16 (8) (2017) 864–873, https://doi.org/10.1038/nmat4917.
[29] H.M. Powell, K.L. McFarland, D.L. Butler, D.M. Supp, S.T. Boyce, Uniaxial strain regulates morphogenesis, gene expression, and tissue strength in engineered skin, Tissue Eng. 16 (3) (2010) 1083–1092, https://doi.org/10.1089/ten.tea.2009.0542.
[30] R. Gauvin, R. Parenteau-Bareil, D. Larouche, H. Marcoux, F. Bisson, A. Bonnet, F. A. Auger, S. Bolduc, L. Germain, Dynamic mechanical stimulations induce anisotropy and improve the tensile properties of engineered tissues produced without exogenous scaffolding, Acta Biomater. 7 (9) (2011) 3294–3301, https://doi.org/10.1016/j.actbio.2011.05.034.
[31] R.E. De Filippo, A. Atala, Stretch and growth: the molecular and physiologic influences of tissue expansion, Plast. Reconstr. Surg. 109 (7) (2002) 2450–2462.
[32] A.E. Ehret, K. Bircher, A. Stracuzzi, V. Marina, M. Zündel, E. Mazza, Inverse poroelasticity as a fundamental mechanism in biomechanics and mechanobiology, Nat. Commun. 8 (1) (2017) 1002, https://doi.org/10.1038/s41467-017-00801-3.
[33] A. Wahlsten, M. Pensalfini, A. Stracuzzi, G. Restivo, R. Hopf, E. Mazza, On the compressibility and poroelasticity of human and murine skin, Biomech. Model. Mechanobiol. 18 (4) (2019) 1079–1093, https://doi.org/10.1007/s10237-019-01129-1.
[34] D.E. Discher, P.A. Janmey, Y.-l. Wang, Tissue cells feel and respond to the stiffness of their substrate, Science 310 (5751) (2005) 1139–1143, https://doi.org/10.1126/science.1116995.
[35] V.F. Achterberg, L. Buscemi, H. Diekmann, J. Smith–Clerc, H. Schwengler, J. J. Meister, H. Wenck, S. Gallinat, B. Hinz, The nano-scale mechanical properties of the extracellular matrix regulate dermal fibroblast function, J. Invest. Dermatol. 134 (7) (2014) 1862–1872, https://doi.org/10.1038/jid.2014.90.

[36] E. Hadjipanayi, V. Mudera, R.A. Brown, Close dependence of fibroblast proliferation on collagen scaffold matrix stiffness, J Tissue Eng. Regen. Med. 3 (2009) 77–84, https://doi.org/10.1002/term.136.

[37] C.P. Ng, B. Hinz, M.A. Swartz, Interstitial fluid flow induces myofibroblast differentiation and collagen alignment in vitro, J. Cell Sci. 118 (20) (2005) 4731–4739, https://doi.org/10.1242/jcs.02605.

[38] S. Mizuno, S. Watanabe, T. Takagi, Hydrostatic fluid pressure promotes cellularity and proliferation of human dermal fibroblasts in a three-dimensional collagen gel/sponge, Biochem. Eng. J. 20 (2–3) (2004) 203–208, https://doi.org/10.1016/j.bej.2003.09.019.

[39] W. Buerzle, C.M. Haller, M. Jabareen, J. Egger, A.S. Mallik, N. Ochsenbein-Koelble, M. Ehrbar, E. Mazza, Multiaxial mechanical behavior of human fetal membranes and its relationship to microstructure, Biomech. Model. Mechanobiol. 12 (4) (2013) 747–762, https://doi.org/10.1007/s10237-012-0438-z.

[40] R. Hopf, L. Bernardi, J. Menze, M. Zündel, E. Mazza, A.E. Ehret, Experimental and theoretical analyses of the age-dependent large-strain behavior of Sylgard 184 (10:1) silicone elastomer, J. Mech. Behav. Biomed. Mater. 60 (2016) 425–437, https://doi.org/10.1016/j.jmbbm.2016.02.022.

[41] L. Bernardi, E. Mazza, A.E. Ehret, The effect of clamping conditions on tearing energy estimation for highly stretchable materials, Eng. Fract. Mech. 188 (2018) 300–308, https://doi.org/10.1016/j.engfracmech.2017.08.035.

[42] T. Biedermann, L. Pontiggia, S. Böttcher–Haberzeth, S. Tharakan, E. Braziulis, C. Schiestl, M. Meuli, E. Reichmann, Human eccrine sweat gland cells can reconstitute a stratified epidermis, J. Invest. Dermatol. 130 (8) (2010) 1996–2009, https://doi.org/10.1038/jid.2010.83.

[43] K.H. Jones, J.A. Senft, An improved method to determine cell viability by simultaneous staining with fluorescein diacetate-propidium iodide, J. Histochem. Cytochem. 33 (1) (1985) 77–79.

[44] A.D. Armour, H.M. Powell, S.T. Boyce, Fluorescein diacetate for determination of cell viability in tissue-engineered skin, Tissue Eng. C Methods 14 (1) (2008) 89–96, https://doi.org/10.1089/tec.2007.0228.

[45] G. Bradski, The OpenCV Library, Dr. Dobb's Journal of Software Tools.

[46] C.W. Smith, R.J. Wootton, K.E. Evans, Interpretation of experimental data for Poisson's ratio of highly nonlinear materials, Exp. Mech. 39 (4) (1999) 356–362, https://doi.org/10.1007/BF02329817.

[47] R. Rezakhaniha, A. Agianniotis, J.T.C. Schrauwen, A. Griffa, D. Sage, C.V. C. Bouten, F.N. Van De Vosse, M. Unser, N. Stergiopulos, Experimental investigation of collagen waviness and orientation in the arterial adventitia using confocal laser scanning microscopy, Biomech. Model. Mechanobiol. 11 (3–4) (2012) 461–473, https://doi.org/10.1007/s10237-011-0325-z.

[48] T. Nolan, R.E. Hands, S.A. Bustin, Quantification of mRNA using real-time RT-PCR, Nat. Protoc. 1 (3) (2006) 1559–1582, https://doi.org/10.1038/nprot.2006.236.

[49] D. Svec, A. Tichopad, V. Novosadova, M.W. Pfaffl, M. Kubista, How good is a PCR efficiency estimate: recommendations for precise and robust qPCR efficiency assessments, Biomol. Detect, Quantif 3 (2015) 9–16, https://doi.org/10.1016/j.bdq.2015.01.005.

[50] X. Rao, X. Huang, Z. Zhou, X. Lin, An improvement of the 2(-delta delta ct) method for quantitative real-time polymerase chain reaction data analysis, Biostat. Bioinforma. Biomath. 3 (3) (2013) 71–85.

[51] M.W. Pfaffl, A new mathematical model for relative quantification in real-time RT-PCR, Nucleic Acids Res. 29 (9) (2001) 2002–2007.

[52] M. Pensalfini, A.E. Ehret, S. Stüdeli, D. Marino, A. Kaech, E. Reichmann, E. Mazza, Factors affecting the mechanical behavior of collagen hydrogels for skin tissue engineering, J. Mech. Behav. Biomed. Mater. 69 (2017) 85–97, https://doi.org/10.1016/j.jmbbm.2016.12.004.

[53] B.A. Roeder, K. Kokini, S.L. Voytik–Harbin, Fibril microstructure affects strain transmission within collagen extracellular matrices, J. Biomech. Eng. 131 (3) (2009) 1–11, https://doi.org/10.1115/1.3005331.

[54] D. Vader, A. Kabla, D. Weitz, L. Mahadevan, Strain-induced alignment in collagen gels, PloS One 4 (6) (2009), e5902, https://doi.org/10.1371/journal.pone.0005902.

[55] T. Panciera, L. Azzolin, M. Cordenonsi, S. Piccolo, Mechanobiology of YAP and TAZ in physiology and disease, Nat. Rev. Mol. Cell Biol. 18 (12) (2017) 758–770, https://doi.org/10.1038/nrm.2017.87.

[56] S. Piccolo, S. Dupont, M. Cordenonsi, The biology of YAP/TAZ: hippo signaling and beyond, Physiol. Rev. 94 (4) (2014) 1287–1312, https://doi.org/10.1152/physrev.00005.2014.

[57] A.S. Curtis, G.M. Seehar, The control of cell division by tension or diffusion, Nature 274 (5666) (1978) 52–53, https://doi.org/10.1038/274052a0.

[58] R.A. Brown, M. Wiseman, C.B. Chuo, U. Cheema, S.N. Nazhat, Ultrarapid engineering of biomimetic materials and tissues: fabrication of nano- and microstructures by plastic compression, Adv. Funct. Mater. 15 (11) (2005) 1762–1770, https://doi.org/10.1002/adfm.200500042.

[59] B. Hinz, D. Mastrangelo, C.E. Iselin, C. Chaponnier, G. Gabbiani, Mechanical tension controls granulation tissue contractile activity and myofibroblast differentiation, Am. J. Pathol. 159 (3) (2001) 1009–1020, https://doi.org/10.1016/S0002-9440(10)61776-2.

[60] J.J. Tomasek, G. Gabbiani, B. Hinz, C. Chaponnier, R.A. Brown, Myofibroblasts and mechano-regulation of connective tissue remodelling, Nat. Rev. Mol. Cell Biol. 3 (5) (2002) 349–363, https://doi.org/10.1038/nrm809.

[61] F. Grinnell, Fibroblast biology in three-dimensional collagen matrices, Trends Cell Biol. 13 (5) (2003) 264–269, https://doi.org/10.1016/S0962-8924(03)00057-6.

[62] R. Kuang, Z. Wang, Q. Xu, S. Liu, W. Zhang, Influence of mechanical stimulation on human dermal fibroblasts derived from different body sites, Int. J. Clin. Exp. Med. 8 (5) (2015) 7641–7647.

[63] S. Yano, M. Komine, M. Fujimoto, H. Okochi, K. Tamaki, Mechanical stretching in vitro regulates signal transduction pathways and cellular proliferation in human epidermal keratinocytes, J. Invest. Dermatol. 122 (3) (2004) 783–790, https://doi.org/10.1111/j.0022-202X.2004.22328.x.

[64] B.W. Benham–Pyle, B.L. Pruitt, W.J. Nelson, Mechanical strain induces E-cadherin-dependent Yap1 and β-catenin activation to drive cell cycle entry, Science 348 (6238) (2015) 1024–1027, https://doi.org/10.1126/science.aaa4559.

[65] W. Li, B.E. Sumpio, Strain-induced vascular endothelial cell proliferation requires PI3K-dependent mTOR-4E-BP1 signal pathway, Am. J. Physiol. Cell Physiol. 288 (4) (2005) H1591–H1597, https://doi.org/10.1152/ajpheart.00382.2004.

[66] C.C. Berry, J.C. Shelton, D.L. Bader, D.A. Lee, Influence of external uniaxial cyclic strain on oriented fibroblast-seeded collagen gels, Tissue Eng. 9 (4) (2003) 613–624, https://doi.org/10.1089/107632703768247313.

[67] K. Webb, R.W. Hitchcock, R.M. Smeal, W. Li, S.D. Gray, P.A. Tresco, Cyclic strain increases fibroblast proliferation, matrix accumulation, and elastic modulus of fibroblast-seeded polyurethane constructs, J. Biomech. 39 (6) (2006) 1136–1144, https://doi.org/10.1016/j.jbiomech.2004.08.026.

[68] A. Livne, E. Bouchbinder, B. Geiger, Cell reorientation under cyclic stretching, Nat. Commun. 5 (2014) 3938, https://doi.org/10.1038/ncomms4938.

[69] E.J. Lee, J.W. Holmes, K.D. Costa, Remodeling of engineered tissue anisotropy in response to altered loading conditions, Ann. Biomed. Eng. 36 (8) (2008) 1322–1334, https://doi.org/10.1007/s10439-008-9509-9.

[70] K. Chen, A. Vigliotti, M. Bacca, R.M. McMeeking, V.S. Deshpande, J.W. Holmes, Role of boundary conditions in determining cell alignment in response to stretch, Proc. Natl. Acad. Sci. Unit. States Am. 115 (5) (2018) 986–991, https://doi.org/10.1073/pnas.1715059115.

[71] J. Foolen, V.S. Deshpande, F.M. Kanters, F.P. Baaijens, The influence of matrix integrity on stress-fiber remodeling in 3D, Biomaterials 33 (30) (2012) 7508–7518, https://doi.org/10.1016/j.biomaterials.2012.06.103.

[72] C. Obbink–Huizer, J. Foolen, C.W.J. Oomens, M. Borochin, C.S. Chen, C.V. C. Bouten, F.P.T. Baaijens, Computational and experimental investigation of local stress fiber orientation in uniaxially and biaxially constrained microtissues, Biomech. Model. Mechanobiol. 13 (5) (2014) 1053–1063, https://doi.org/10.1007/s10237-014-0554-z.

[73] A. Saez, M. Ghibaudo, A. Buguin, P. Silberzan, B. Ladoux, Rigidity-driven growth and migration of epithelial cells on microstructured anisotropic substrates, Proc. Natl. Acad. Sci. Unit. States Am. 104 (20) (2007) 8281–8286, https://doi.org/10.1073/pnas.0702259104.

[74] J.G. Rheinwald, H. Green, Serial cultivation of strains of human epidermal keratinocytes: the formation of keratinizing colonies from single cells, Cell 6 (3) (1975) 331–343, https://doi.org/10.1016/S0092-8674(75)80001-8.

[75] F.A. Auger, M. Rouabhia, F. Goulet, F. Berthod, V. Moulin, L. Germain, Tissue-engineered human skin substitutes developed from collagen-populated hydrated gels: clinical and fundamental applications, Med. Biol. Eng. Comput. 36 (6) (1998) 801–812, https://doi.org/10.1007/BF02518887.

[76] P. Young, O. Boussadia, H. Halfter, R. Grose, P. Berger, D.P. Leone, H. Robenek, P. Charnay, R. Kemler, U. Suter, E-cadherin controls adherens junctions in the epidermis and the renewal of hair follicles, EMBO J. 22 (21) (2003) 5723–5733, https://doi.org/10.1093/emboj/cdg560.

[77] F.M. Watt, Role of integrins in regulating epidermal adhesion, growth and differentiation, EMBO J. 21 (15) (2002) 3919–3926, https://doi.org/10.1093/emboj/cdf399.

[78] F.M. Watt, P.H. Jones, Expression and function of the keratinocyte integrins, Development 119 (1993) 185–192.

[79] Y. Wang, G. Wang, X. Luo, J. Qiu, C. Tang, Substrate stiffness regulates the proliferation, migration, and differentiation of epidermal cells, Burns 38 (3) (2012) 414–420, https://doi.org/10.1016/j.burns.2011.09.002.

[80] F. N. Kenny, Z. Drymoussi, R. Delaine-Smith, A. P. Kao, A. C. Laly, M. M. Knight, M. P. Philpott, J. T. Connelly, Tissue stiffening promotes keratinocyte proliferation through activation of epidermal growth factor signaling, J. Cell Sci. 131 (10). doi: 10.1242/jcs.215780.

[81] M. Aragona, A. Sifrim, M. Malfait, Y. Song, J. Van Herck, S. Dekoninck, S. Gargouri, G. Lapouge, B. Swedlund, C. Dubois, P. Baatsen, K. Vints, S. Han, F. Tissir, T. Voet, B.D. Simons, C. Blanpain, Mechanisms of stretch-mediated skin expansion at single-cell resolution, Nature 584 (7820) (2020) 268–273, https://doi.org/10.1038/s41586-020-2555-7.

[82] E.N. Lamme, R.T. Van Leeuwen, K. Brandsma, J. Van Marie, E. Middelkoop, Higher numbers of autologous fibroblasts in an artificial dermal substitute improve tissue regeneration and modulate scar tissue formation, J. Pathol. 190 (5) (2000) 595–603, https://doi.org/10.1002/(SICI)1096-9896(200004)190:5<595::AID-PATH572>3.0.CO;2-V.

[83] S. Ruijtenberg, S. van den Heuvel, Coordinating cell proliferation and differentiation: antagonism between cell cycle regulators and cell type-specific gene expression, Cell Cycle 15 (2) (2016) 196–212, https://doi.org/10.1080/15384101.2015.1120925.